Journal of Controlled Release 371 (2024) 1–15

Contents lists available at ScienceDirect

Journal of Controlled Release

journal homepage: www.elsevier.com/locate/jconrel

Phospholipids of inhaled liposomes determine the *in vivo* fate and therapeutic effects of salvianolic acid B on idiopathic pulmonary fibrosis

Jianqing Peng [a,1], Qin Wang [a,1], Runbin Sun [d], Ke Zhang [c], Yi Chen [a,*], Zipeng Gong [a,b,**]

[a] State Key Laboratory of Functions and Applications of Medicinal Plants, School of Pharmaceutical Sciences, Guizhou Medical University, Guizhou 561113, China
[b] Guizhou Provincial Key Laboratory of Pharmaceutics, School of Pharmaceutical Sciences, Guizhou Medical University, Guizhou 561113, China
[c] The Key and Characteristic Laboratory of Modern Pathogenicity Biology, School of Basic Medical Sciences, Guizhou Medical University, Guizhou 561113, China
[d] Nanjing Drum Tower Hospital, the Affiliated Hospital of Nanjing University Medical School, Nanjing 210008, China

ARTICLE INFO

Keywords:
Phospholipid
Liposomes
Salvianolic acid B
Inhalation
Idiopathic pulmonary fibrosis

ABSTRACT

Since phospholipids have an important effect on the size, surface potential and hardness of liposomes that decide their *in vivo* fate after inhalation, this research has systematically evaluated the effect of phospholipids on pulmonary drug delivery by liposomes. In this study, liposomes composed of neutral saturated/unsaturated phospholipids, anionic and cationic phospholipids were constructed to investigate how surface potential and the degree of saturation of fatty acid chains determined their mucus and epithelium permeability both *in vitro* and *in vivo*. Our results clearly indicated that liposomes composed of saturated neutral and anionic phospholipids possessed high stability and permeability, compared to that of liposomes composed of unsaturated phospholipids and cationic phospholipids. Furthermore, both *in vivo* imaging of fluorescence-labeled liposomes and biodistribution of salvianolic acid B (SAB) that encapsulated in liposomes were performed to estimate the effect of phospholipids on the lung exposure and retention of inhaled liposomes. Finally, inhaled SAB-loaded liposomes exhibited enhanced therapeutic effects in a bleomycin-induced idiopathic pulmonary fibrosis mice model *via* inhibition of inflammation and regulation on coagulation-fibrinolytic system. Such findings will be beneficial to the development of inhalable lipid-based nanodrug delivery systems for the treatment of respiratory diseases where inhalation is the preferred route of administration.

1. Introduction

Idiopathic pulmonary fibrosis (IPF) is a chronic, progressive interstitial pulmonary fibrosis disease of the lower respiratory tract. Its pathological characteristics are excessive accumulation of fibroblasts and myofibroblasts, abnormal deposition of extracellular matrix, and destruction of alveoli, resulting in restrictive ventilation disorders, abnormal arterial blood gases and hypoxemia. Clinically, the median survival time of patients is 2 to 5 years, indicating high mortality of IPF [1,2]. Currently, oral pirfenidone and nintedanib are clinically approved for the treatment of mild to moderate IPF. However, this treatment regimen can only delay the progression of pulmonary fibrosis but cannot completely prevent the decline of lung function. Lung transplantation is proven to be the only clinical therapeutic strategy to effectively prolong the survival time of patients. Unfortunately, lung transplantation is poorly applicated by patients due to high treatment costs, lack of matched donors, and postoperative rejection [3–5]. Therefore, clinical treatment of IPF still faces challenges of poor prognosis and short survival, and there is an urgent need to develop new treatment options.

Although the cause of IPF has not yet been determined, increasing evidence suggests that alveolar epithelial damage and abnormal wound repair are key factors in the development of IPF [3]. Sustained injury to alveolar epithelial cells leads to disruption of epithelial-fibroblast communication, and epithelial cells release a variety of pro-fibrotic cytokines, ultimately leading to the recruitment and activation of myofibroblasts and fibroblasts, which secrete excess collagen-rich extracellular matrix (ECM). Excessive accumulation of ECM renders the collapse and dysfunction of alveoli resulting in reduced gas exchange

* Corresponding author.
** Corresponding author at: State Key Laboratory of Functions and Applications of Medicinal Plants, School of Pharmaceutical Sciences, Guizhou Medical University, Guizhou 561113, China.
E-mail addresses: chenyi@gmc.edu.cn (Y. Chen), gzp4012607@gmc.edu.cn (Z. Gong).
[1] Jianqing Peng and Qin Wang contributed equally to this work.

https://doi.org/10.1016/j.jconrel.2024.05.026
Received 6 December 2023; Received in revised form 18 April 2024; Accepted 15 May 2024
Available online 21 May 2024

and respiratory distress, which is ultimately life-threatening [6,7]. Besides, IPF patients exhibit fibrin accumulation in the alveoli accompanied by thrombus formation [8]. Studies have shown that thrombin, activated coagulation factor X (FXa), and plasmin play important roles in the pathogenesis of pulmonary fibrosis. In the early stages of lung tissue injury, it is often accompanied by a coagulation cascade, activation of platelets, and local secretion of soluble substances, which in turn leads to increased vascular permeability. Prothrombin and plasmin factors can enter the damaged lung parenchymal tissue through blood circulation and participate in the process of coagulation and fibrinolysis [8–11]. Collectively, both collagen accumulation and coagulation-fibrinolytic system regulation is required in the treatment of IPF.

Salvianolic acid B (SAB) is a water-soluble component of *Salvia miltiorrhiza* Bunge and is a potential drug for the treatment of IPF. Previous studies have shown that SAB can effectively inhibit pulmonary fibrosis by reducing collagen expression, reducing inflammatory cell infiltration, down regulating pro-inflammatory cytokine secretion and oxidative stress levels [12–15]. Noteworthy, SAB can effectively inhibit the activation of coagulation factors, prevent thrombin activation, upregulate plasminogen activator (PA) and inhibit the expression of plasminogen activator inhibitor-1 (PAI-1), which results in the conversion of plasminogen to plasmin and activation of the fibrinolytic system [14,16]. Therefore, SAB is an effective drug for the treatment of IPF *via* hydrolysis of collagen and fibronectin. For the clinical treatment of IPF, inhalation of SAB aerosol solution is a promising way of administration. Compared with the intravenous injection and oral administration, inhalation can quickly reach the respiratory tract and lung and increase the concentration of the drug in the lung, leading to rapid onset of action, less systemic exposure, and good compliance. Hence, inhalation is widely recommended for the treatment of respiratory diseases, especially for drugs that are prone to hepatic metabolism after oral administration [17,18]. However, inhalation of SAB aerosol solution might encounter a series of physiological barriers in the respiratory tract and lung resulting in reduced lung exposure and retention of SAB, thus affecting the therapeutic effect on IPF. Specifically, SAB might interact with mucus in the conducting airways and be cleared by the cilia of respiratory epithelial cells through the oropharynx excretion. In the pulmonary alveoli, SAB is prone to cross the air-blood barrier quickly *via* paracellular pathway and enter the circulation, which reduces drug accumulation in the lungs and increases systemic exposure of SAB [17–20]. It is necessary to prolong the residence time of SAB in the alveoli and increase the uptake by alveolar epithelial cells as well as macrophages for ideal therapeutic effect on IPF.

Liposome is one of the most used nanocarrier for drugs to prepare the aerosol inhalation solution due to its excellent biocompatibility, high colloidal stability, flexible surface modification and one of the most developed nanomedicines in clinic practice. Studies have shown that liposomal drugs can prolong the residence time in the lung after inhalation, enhance the local therapeutic effect, and reduce systemic exposure [21–24]. Currently, the FDA has approved Arikayce® (liposomal amikacin inhalation suspension) for the treatment of pulmonary disease caused by *mycobacterium avium* complex (MAC) infection. In addition, Linhaliq™ (liposomal ciprofloxacin), Lipoquin® (liposomal ciprofloxacin) and Pulmaquin® (liposomal ciprofloxacin) developed by Aradigm Corporation are used to treat *pseudomonas aeruginosa*-induced lung infection [25,26]. Liposomes will encounter complex pulmonary microenvironment after inhalation, including mucociliary clearance and pulmonary surfactant-mediated macrophage phagocytosis. The size, hardness, and surface properties of liposomes all affect their ability to overcome physiological barriers in the respiratory tract and lung [27]. Most current research focused on using surface modification strategies to improve the efficiency of the pulmonary delivery of liposomes after inhalation. Polyethylene glycol (PEG) as the most commonly used surface modification material can effectively increase the mucus permeability of liposomes [28,29]. We used a variety of polysaccharides for surface modification to improve the mucus penetration and lung retention capabilities of liposomes in the previous studies [30–32]. In addition to liposome surface modification, the type of phospholipid constituting liposomes will also significantly affect the size, structure, and surface properties of liposomes, thereby affecting the pulmonary retention of drugs and their therapeutic effects on IPF after inhalation. However, the effects of the degrees of fat chain saturation and the electrical properties of polar parts of phospholipids on the pulmonary delivery efficacy of liposomes after inhalation have been rarely discussed.

In this study, neutral saturated/unsaturated phospholipids (SPC, HSPC, DPPC), anionic phospholipids (DPPG) and cationic phospholipids (DOTAP) have been used to construct SAB-loaded liposomes, respectively. We studied the interactions between liposomes and mucin, then evaluated the permeability of mucus and epithelial cells, as well as the cellular uptake of liposomes by epithelial cells and macrophages. To explore the biodistribution of liposomes after inhalation, we observed the biodistribution of DiR-labeled liposomes by *in vivo* imaging systems and detected the disposition of SAB in different region of lung after inhalation of SAB-loaded liposomes. A bleomycin sulfate (BLM)-induced pulmonary fibrosis mouse model was established to systematically evaluate the therapeutic effects of SAB-loaded liposomes on IPF (Fig. 1).

2. Materials and methods

2.1. Materials and reagents

Soybean phospholipid (SPC, purity CS-95, Lot No. SY-SI-190601) and hydrogenated soybean phosphatidylcholine (HSPC, Lot No. B60455) were obtained from A.V.T Pharmaceutical Co., Ltd. (Shanghai, China). 1,2-dipalmitoyl-sn-glycero-3-phosphocholine (DPPC, Lot No. RA0221346), 1,2-dipalmitoyl-sn-glycero-3-phospho-(1-rac-glycerol) (DPPG, Lot No. RA0212501), (2,3-dioleoyloxy-propyl)-trimethylammonium-chloride (DOTAP, Lot No. RO0210801), and 1,2-distearoyl-sn-glycero-3-phosphoethanolamine-N-(polyethylene glycol)-2000 (DSPE-PEG2000, Lot No. RS0200412) were purchased from Xi'an Ruixi Biological Technology Co., Ltd. (Xi'an, China). Cholesterol (Chol, VetecTM reagent grade, purity ≥92.5%, Lot No. WXBB1238) was purchased from Sigma-aldrich (Shanghai, China). Egg yolk emulsion (purity 50%, Lot No. 20221130) was provided by Hopebio Biotechnology Co., Ltd. (Qingdao, China). Gastric mucin (derived from pigs, Lot No. J1202A) was from Dalian Meilun Biotechnology Co., Ltd. (Liaoning, China). Salvianolic acid B (SAB, purity 98%, Lot No. C15272235), diethylenetriaminepentaacetic acid (DTPA, purity ≥99%, Lot No. C14854636), Nile red (NR, purity ≥96%, Lot No. C12057927), 3-hydroxyisoquinoline (HIQ, purity 97%, Lot No. C11223845), rhodamine B (RB, purity ≥99%, Lot No.C10006604), DiR (purity ≥95%, Lot No. C13337722), bleomycin sulfate (BLM, purity 1.5–2.0 units/mg, Lot No. C13578600), trans-cinnamic acid (CA, purity 99%, Lot No. C13149213), L-ascorbic acid (purity > 99%, Lot No. C14776339), and inorganic chemicals and organic solvents of analytical grade were obtained from Macklin Biochemical Co., Ltd. (Shanghai, China). HYP kit (Lot No. 0428A23), TGF-β1 ELISA kit (Lot No. Apr 2023), TNF-α ELISA kit (Lot No. Apr 2023), IL-1β ELISA kit (Lot No. Apr 2023), IL-6 ELISA kit (Lot No. Oct 2022), FXa ELISA kit (Lot No. Sep 2023), FIIa ELISA kit (Lot No. Sep 2023), FDP ELISA kit (Lot No. Sep 2023), PAI-1 ELISA kit (Lot No. Jun 2023), uPA ELISA kit (Lot No. Jun 2023) and tPA ELISA kit (Lot No. Jun 2023) were provided by Shanghai zcibio technology Co., Ltd. (Shanghai, China). Cell counting kit-8 (Lot No. K101828133EF5E) was purchased from APExBio Technology LLC (Shanghai, China).

2.2. Animals and cell cultures

C57BL/6 J mice (20 ± 2 g, 6–8 weeks old) and KM mice (20 ± 2 g, 6–8 weeks old) were obtained from the Experimental Animal Center of Guizhou Medical University. All animal care and experiments were approved by the Animal Welfare and Ethics Committee of Guizhou

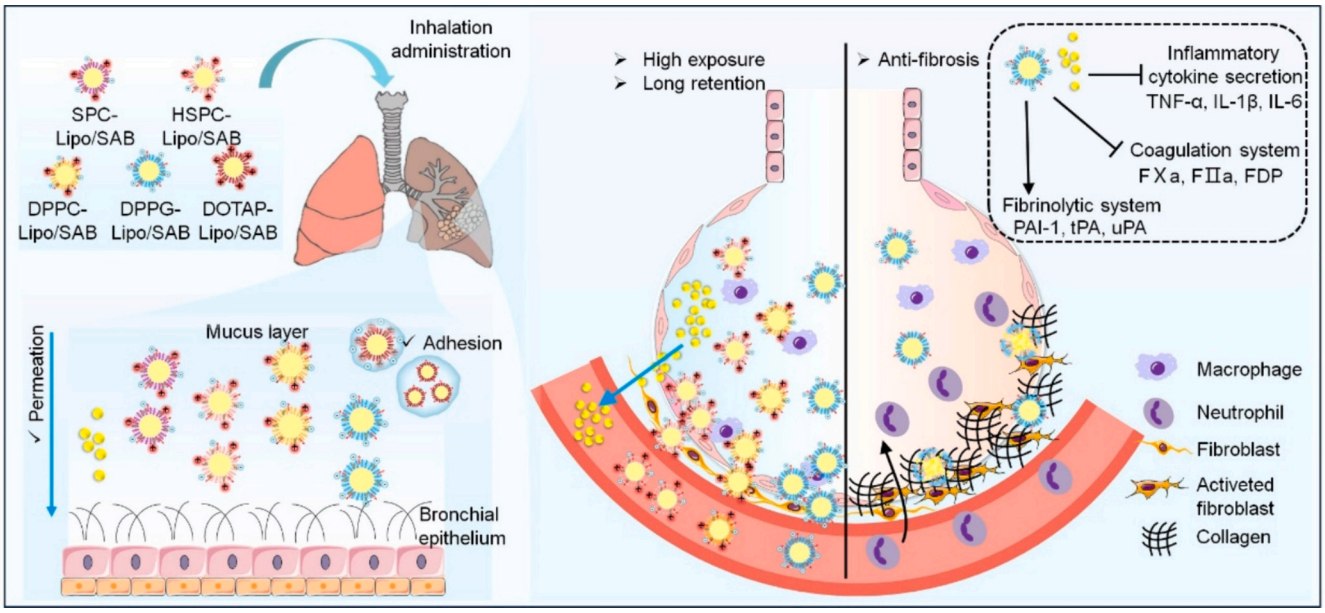

Fig. 1. Schematic illustration of the *in vivo* fate of SAB-loaded liposomes after inhalation and their therapeutic effects and mechanisms on IPF.

Medical University (No: 2303256). Mice were housed at room temperature (23 ± 2 °C) and constant humidity (45 ± 10%) under SPF conditions. Animals were acclimated for one week before starting experiments.

A549 cells, RAW264.7 cells, and HBE135-E6E7 cells were purchased from Procell Life Technology Co., Ltd. (Wuhan, China). A549 cells were cultured in RPMI1640 (Gibco, Lot No. 8123326) supplemented with 10% fetal bovine serum (FBS, Cellmax, Lot No. 20221220) and 1% penicillin/streptomycin (P/S, Cellmax, Lot No. 20220810). RAW264.7 cells were cultured in DMEM (Cellmax, Lot No. 20221029) supplemented with 10% FBS and 1% P/S. HBE135-E6E7 cells were cultured in epithelial cell growth medium (Procell Life Technology Co., Ltd., Lot No. WH3123U184) supplemented with epithelial cell growth additive, 2% FBS and 1% P/S. Cells were maintained at 37 °C in a humidified atmosphere containing 5% CO_2, and the cell medium was changed every other day.

2.3. Preparation of SAB-loaded liposomes

Liposomes were prepared by the thin film dispersion method followed by the pH gradient method with slightly modified methods [33]. Briefly, SPC: Chol: DSPE-PEG2000 or HSPC: Chol: DSPE-PEG2000 or DPPC: Chol: DSPE-PEG2000 or DPPC: DPPG: Chol: DSPE-PEG2000 or DOTAP: DPPC: Chol: DSPE-PEG2000 were dissolved with chloroform: methanol (50: 1, *v/v*) mixture in a certain ratio. And the organic mixture was rotary-evaporated (RE-52AA, Beidi Experimental Instrument Co., Ltd., Nanjing, China) under reduced pressure at 40 °C to form a uniform thin-film. The film was further dried under vacuum for 30 min to remove residual organic solvent. Next, the lipid film was subsequently hydrated with PBS at 50 °C for 30 min until the thin-film was completely off. The suspension was sonicated (ultrasonic 3 s, interval 3 s, power 200 W) for 3 min using an ultrasonic cell disrupter (Beidi-650E, Beidi Experimental Instrument Co., Ltd., Nanjing, China), and filtered through 0.45 μm micro porous membrane to obtain blank liposomes. Then SAB was dissolved in 1% glycine-HCl buffer (pH 3.3) and added dropwise to the preformed blank liposomes according to the mass ratio of phospholipid: SAB = 10: 1, and incubated at 50 °C for 10 min, followed by immediate cooling in an ice bath. The resulting SAB-loaded liposomes were purified by dialysis against PBS (MWCO, 3500 Da) to remove unencapsulated SAB.

DiR-labeled liposomes and förster resonance energy transfer (FRET) reagents: 3-hydroxyisoquinoline (HIQ) and nile red (NR) co-loaded liposomes are prepared by dissolving the fluorescein in a mixture of chloroform and methanol to form the thin film, while rhodamine B (RB)-loaded liposomes are prepared by dissolving RB in the hydration medium. The other steps are the same with the preparation of SAB-loaded liposomes.

2.4. Characterization of SAB-loaded liposomes

The morphology of SAB-loaded liposomes was observed by transmission electron microscope (TEM, Tecnai 12, Philips, Holland, Amsterdam, Netherlands). The particle size, polydispersity (PDI), and zeta potential of SPC-Lipo/SAB, HSPC-Lipo/SAB, DPPC-Lipo/SAB, DPPG-Lipo/SAB and DOTAP-Lipo/SAB were measured by NanoBrook 90Plus PALS (Brookhaven, GA, USA). The concentration of SAB in liposomal preparations was measured by high performance liquid chromatography (HPLC), which used Shimadzu LC-16 (Suzhou, China) with a UV detector (SPD-16, Shimadzu, Suzhou, China) using a reversed phase column (Welch, Ultimate® ODS-3, 4.6 × 250 mm, 5 μm, Huaian, China), at 30 °C. A mobile phase consisted of acetonitrile and 0.1% phosphoric acid (30: 70, *v/v*) at a flow rate of 1 mL/min and detecting at the wavelength of 286 nm. The drug loading efficiency (LE) and drug loading capacity (DL) were calculated by the following eqs. (1) and (2):

$$LE\ (\%) = \frac{W_{drug\ loaded}}{W_{drug\ added}} \times 100\% \quad (1)$$

$$DL\ (\%) = \frac{W_{drug\ loaded}}{W_{total\ liposome}} \times 100\% \quad (2)$$

Then dialysis method was used to determine the *in vitro* release of SAB. A dialysis bag (MWCO, 14 kDa) holding 1 mL of SAB-loaded liposomal preparations or the mixture of liposomal preparations and artificial mucus was immersed in 15 mL of PBS in a capped bottle and incubated at 37 °C with stirring at a speed of 50 rpm. The content of SAB released into the medium was determined using the HPLC method described above. To determine the stability of the formulations, SAB-loaded liposomes were kept in an incubator at 4 °C and the particle size, PDI and zeta potential were measured for one week.

2.5. In vitro stability of SAB-loaded liposomes in mucus and bronchoalveolar lavage fluid (BALF)

FRET is a photophysical process that has been used to investigate the stability and release kinetics of nanoparticles that are sensitive to distance changes. When the donor and acceptor fluorophores have a large spectral overlap in their excitation and emission spectra and are within 10 nm of each other, energy transfer occurs between them. The donor fluorophore in the excited state transfers energy to the acceptor, resulting in acceptor fluorescence [34,35]. The stability of liposomes prepared with different phospholipids in PBS solution, 0.2% (*w/v*) mucin solution, BALF was evaluated by FRET. As previously described, artificial mucus was prepared by adding 250 μL of sterile egg yolk emulsion, 250 mg of mucin, 0.295 mg of DTPA, 250 mg of sodium chloride, 110 mg of potassium chloride, and 1 mL of RPMI 1640 to 50 mL distilled water [36]. To obtain BALF, KM mice (20 ± 2 g, 6–8 weeks old) were euthanized. The neck trachea of mice was surgically isolated and cut, a cannula was inserted and fixed in place. Bronchoalveolar lavage was repeated three times with 2 mL of ice-cold PBS through tracheal intubation to obtain BALF. The obtained BALF was centrifuged (350 ×*g*, 10 min) at 4 °C to remove cells and the supernatant was collected. For the analysis, 0.5 mL of HIQ and NR co-loaded liposomes were added to 2 mL of PBS and lung-relevant media. The samples were incubated at 37 °C, the maximum emission band intensity was detected at $\lambda_{Ex}/\lambda_{Em}$ = 400/635 nm, and the particle size changes of HIQ and NR co-loaded liposomes were monitored at pre-determined time intervals. The FRET signal was represented by calculating the peak intensity ratio of the acceptor fluorescence before and after the treatment (I/I_0). The decrease of the emission ratio and change of particle size were considered indicative of disassembly/aggregation.

2.6. Interactions between SAB-loaded liposomes and mucin/BALF

2.6.1. Turbidity measurement by UV–visible spectrophotometry

The interactions between mucin and liposomes were examined by turbidimetric measurements using a UV–visible spectrophotometer [37]. Briefly, equal volumes of mucin and SAB-loaded liposomes composed of different phospholipids were mixed at different mass ratios (0.031, 0.125, 0.5, 1, 2). Subsequently, these mixtures were incubated at 37 °C for 1 h, and then the absorbance of each system was determined at λ = 500 nm using a spectrophotometer (UV-2700, Shimadzu, Japan) and considered as the effective absorbance (A_{effect}). The absorbance for mucin and the SAB-loaded liposomes individually under the corresponding conditions were also measured and calculated the theoretical absorbance (A_{theory}). The interactions between mucin and the SAB-loaded liposomes can be shown by the difference in absorbance (ΔA), which was calculated as eq. (3):

$$\Delta A = A_{effect} - A_{theory} \tag{3}$$

2.6.2. Particle size and zeta potential measurement

Equal amounts of SAB-loaded liposomes composed of different phospholipids were mixed with mucin solution or BALF in different proportions. The solutions were incubated for 1 h at 37 °C. The particle size and zeta potential of each mixture were measured using a NanoBrook 90Plus PALS. We also examined the influence of different incubation times on the particle size and zeta potential at a fixed ratio.

2.6.3. In vitro penetration of SAB-loaded liposomes through mucus layer

In vitro mucus penetration properties of the different liposomes were evaluated by an artificial mucus model using transwell as reported previously [36,38]. Briefly, the artificial mucus was prepared as described. Then, 150 μL of the above artificial mucus was transferred to each donor chamber of the Transwell® (6.5 mm, pore size 3.0 μm), with 800 μL of pH 7.4 PBS added to the accepter chamber. Thereafter, the transwell was equilibrated at the temperature of 37 °C for 1 h. Then upper layer of the artificial mucus was added with 100 μL of SAB-loaded liposomes composed of different phospholipids. 100 μL of samples in acceptor chamber were withdrawn at specific time intervals at 37 °C and replaced by fresh buffer. At same times, samples were dissolved in methanol to measure SAB content through HPLC. The results were expressed as the permeation percentage of SAB-loaded liposomes that penetrated through the artificial mucus layer. The P_{app} of SAB was calculated according to the following eq. (4):

$$P_{app} = V \times \frac{dC}{dt} \times \frac{1}{A} \times \frac{1}{C_0} \tag{4}$$

Where P_{app} is the apparent permeability coefficient, V is the volume of the receiver compartment. dC/dt is the drug concentrations obtained in the acceptor chamber per unit time (s), namely, the final drug concentration in the acceptor chamber divided by the transport time. A is the surface area of the membrane (cm^2), and C_0 is the initial drug concentration in the donor compartment.

2.7. In vitro cellular uptake and transmembrane transport of liposomes

To study the cellular uptake, HBE135-E6E7 cells, A549 cells and RAW264.7 cells were cultured as previously described and seeded at a density of 2 × 10^5 cells per well in 6-well plates. Thereafter, free SAB and SAB-loaded liposomes (at an equivalent lipid concentration of 0.4 mg/mL) were diluted with serum-free medium and incubated with cells for 2 h and 4 h, respectively. The cells were washed three times with PBS, collected with RIPA buffer (containing 1% PMSF), and split into two aliquots. One aliquot was used for BCA assay to determine the protein concentration, and the other aliquot was extracted with methanol and analyzed by HPLC for the SAB content in cells.

To evaluate the transport behaviors of liposomes *in vitro*, HBE135-E6E7 cell and A549 cell model was established. Briefly, HBE135-E6E7 cells or A549 cells were seeded on transwell inserts (diameter 12 mm, pore size 0.4 μm) at a density of 2.5 × 10^5 cells per well and cultured in a 37 °C incubator with 5% CO_2. SAB-loaded liposomes were added to the donor chamber, and the accepter chamber was filled with 1.0 mL of fresh medium. Samples were taken from the accepter chamber at 4 h. Methanol was added to each sample to extract SAB, and then dried at 40 °C under nitrogen purge. The precipitate was reconstituted with 100 μL of methanol and vortexed to dissolve. Then, 200 μL of a mixed solution of acetonitrile and 0.1% phosphoric acid solution was added. The final solution was centrifugated (9500 ×*g*, 10 min) and the supernatant was used for detection by HPLC. The P_{app} of SAB was calculated. Besides, TEER values were measured to monitor the effect of the SAB preparations on monolayer integrity. The initial TEER values of the cell monolayers were determined. The apical medium was then removed and replaced with SAB-loaded liposomes. At 4 h, the SAB-loaded liposomes were withdrawn from the upper chambers and replaced with culture medium to measure the TEER values of the cell monolayers.

The distribution of RB-loaded liposomes in lung parenchyma was investigated. After anesthesia with isoflurane, mice were intratracheally instilled with 100 μL of RB-labeled liposomes composed of different phospholipids *via* endotracheal intubation (22G surflo®. I. V. Catheter, Terumo Corp, Biñan, Philippines), at an equivalent RB dosage of 100 μg/kg. After 2 h, the mice were sacrificed by cervical dislocation. The trachea and lung tissue were fixed using 4% paraformaldehyde solution for 24 h and embedded in tissue freezing medium. Then, the embedded tissue was frozen sliced into transection with thickness of 10 μm. After staining with DAPI solution (10 μg/mL), the pictures were taken by confocal laser scanning microscope at $\lambda_{Ex}/\lambda_{Em}$ = 405/437 nm for the DAPI and $\lambda_{Ex}/\lambda_{Em}$ = 550/580 nm for the RB.

2.8. Biodistribution of the DiR-labeled liposomes after inhalation

The biodistribution of the liposomes were studied using DiR-labeled liposomes. Briefly, the mice (KM mice, 20 ± 2 g, 6–8 weeks old) were

randomly divided into 4 groups. After anesthesia with isoflurane, 50 μL of DiR-labeled liposomes were administered by inhalation *via* endotracheal intubation (22G surflo®. I. V. Catheter, Terumo Corp, Biñan, Philippines) and free DiR solution was used as a control (at an equivalent DiR dosage of 1 mg/kg). The mice were placed face up, and the fluorescence *in vivo* was measured from the abdomen using an *in vivo* imaging system (IVIS Lumina III, PerkinElmer Inc., USA) at various time points. After anesthesia and dissection at the last time point, the heart, liver, spleen, lung, and kidney were isolated and collected for *ex vivo* imaging ($\lambda_{Ex} = 748$ nm and $\lambda_{Em} = 780$ nm). Set the fluorescence in the lung compartment as the region of interest (ROI) and calculated the fluorescence intensity using Living Image® software of PerkinElmer, Inc.

2.9. Pulmonary retention, pharmacokinetic, and tissue distribution studies

The mice (KM mice, 20 ± 2 g, 6–8 weeks old) were randomly divided into 4 groups: free SAB group, HSPC-Lipo/SAB group, DPPC-Lipo/SAB group and DPPG-Lipo/SAB group. The mice were deprived of food for 12 h prior to the experiment, while having unrestricted access to water. After isoflurane anesthesia, free SAB and SAB-loaded liposomes are administered intratracheally according to the method described in *section 2.8*, at a SAB dose of 5 mg/kg. At predetermined time intervals (0.02, 0.05, 0.08, 0.17, 0.5, 1, 2, 4, 8 h), the mice were anesthetized, the plasma was obtained by speed centrifugation (1160 ×*g*, 10 min) at 4 °C of the collected abdominal aorta blood. After blood collection, bronchoalveolar lavage was repeated three times with 1 mL of ice-cold PBS through tracheal intubation to obtain BALF. Lung and other tissues were quickly removed. The supernatant and sediment of BALF were separated by high-speed centrifugation (9500 ×*g*, 10 min).

2.9.1. BALF supernatant sample processing

Two hundred microliter of the sample was accurately transferred into a centrifuge tube, followed by the addition of 200 μL of methanol. The mixture was vortexed for 2 min and sonicated in a water bath for 15 min. After vortexing, sample was mixed with 10 μL of internal standard (10 μg/mL of cinnamic acid), 10 μL of 1.4 mg/mL L-ascorbic acid and 200 μL of 10% (*v/v*) hydrochloric acid. The mixture was vortexed for another 2 min and then extracted with 1 mL of ethyl acetate. The organic phase was placed in a new centrifuge tube after centrifugation (9500 ×*g*, 10 min), then 1 mL of ethyl acetate was added to the aqueous phase to extract SAB. The above extraction liquid was dried at 40 °C under nitrogen purge. Thereafter, the precipitate was reconstituted with 100 μL of methanol and vortexed to dissolve. Then, 200 μL of a mixed solution of acetonitrile and 0.1% phosphoric acid solution was added. The final solution was centrifugated (9500 ×*g*, 10 min) and the supernatant was used for detection by HPLC.

2.9.2. BALF sediment sample processing

Accurately added 200 μL methanol to the sample and vortexed for 2 min. Then, sonicated in a water bath for 15 min. Ten microliter of internal standard (10 μg/mL of cinnamic acid) was added, and the subsequent processing was the same as that of the BALF supernatant sample.

2.9.3. Plasma sample processing

Two hundred microliter of the plasma sample was added to a centrifuge tube, followed by the addition of 200 μL of methanol. The mixture was vortexed for 2 min and sonicated in a water bath for 15 min. Ten microliter of internal standard (10 μg/mL of cinnamic acid) was added, and the subsequent processing was the same as that of the BALF supernatant sample.

2.9.4. Tissue sample processing

Accurately weighed tissue samples were put into a centrifuge tube, PBS and methanol mixture solution was added according to a fixed ratio, thereafter the samples were fully homogenized. The homogenate was centrifugated at 2080 ×*g* for 10 min, and 400 μL of the supernatant was added into a centrifuge tube. Ten microliter of internal standard (10 μg/mL of cinnamic acid) was added, and the subsequent processing was the same as that of the BALF supernatant sample.

2.10. Treatments on BLM-induced IPF mice model

To establish IPF mice model, C57BL/6 J mice (20 ± 2 g, 6–8 weeks old) were acclimated for one week and then anesthetized with isoflurane. BLM was administered intratracheally at a dose of 3 mg/kg for one time to establish the IPF model. The mice were then shaken and rotated to evenly distribute the fluid in the lungs. After 7 days, they were randomly assigned to nine groups, including control, model, free SAB, blank HSPC-Lipo, blank DPPC-Lipo, blank DPPG-Lipo, HSPC-Lipo/SAB, DPPC-Lipo/SAB, and DPPG-Lipo/SAB, and treated with SAB preparations at an equivalent SAB dosage of 5 mg/kg intratracheally once a day for one week. At the end of this experiment, the mice were anesthetized, and the left main bronchus was ligated. Then the trachea was incised and inserted into a cannula. BALF was collected on the right lung of mice by washing three times with 0.5 mL of ice-cold PBS. The left lung was removed, rinsed with pre-cooled PBS and blotted with filter paper, fixed in 4% paraformaldehyde or stored at −80 °C for histological or pharmacodynamic analysis.

2.11. Hematoxylin and eosin (H&E), Masson's, and immunohistochemistry (IHC) staining

The lungs were fixed with 4% paraformaldehyde for at least 48 h and embedded in paraffin. We prepared sections of lung tissues which stained with H&E and Masson's staining. Lung specimens were stained with α-SMA and collagen-I (Col—I) antibodies using an immunohistochemistry technique. H&E lesions can be divided into 4 levels that was shown in the Table S1 [32,39]. The scope of each lesion is determined by the total score. The images of Masson's staining and IHC were processed semi-quantitatively by Image J.

2.12. Determination of related cytokines in lung tissue and BALF

For the quantification of hydroxyproline (HYP), an appropriate amount of lung tissue was weighed in a glass tube and chopped into small pieces for digestion. The measurement was performed according to the instructions of the HYP kit, and the protein in the sample was extracted separately for quantification. For the measurement of coagulation-fibrinolytic system-related factors, the lung tissue was added to pre-cooled PBS at a ratio of 1: 9 (g: mL) and homogenized thoroughly on ice in a glass homogenizer. The homogenate was centrifuged at 5000 ×*g* for 10 min at 4 °C, and then the supernatant was collected for analysis. ELISA kits were used to detect the levels of activated coagulation factor X (FXa), activated coagulation factor II (FIIa), fibrinogen degradation product (FDP), PAI-1, urokinase type plasminogen activator (uPA) and tissue type plasminogen activator (tPA) in the lung tissue in accordance with the manufacturer's instructions. Besides, the level of TGF-β1, TNF-α, IL-6 and IL-1β in BALF were measured using ELISA kits as well according to the manufacturer's instructions.

2.13. Statistical analysis

The experimental results were expressed as mean ± standard deviation (SD) from sample numbers (*n*). The differences detection of the mean values between multiple groups were determined *via* one-way analysis of variance (ANOVA), with Tukey test. Comparisons between control and model groups were assessed by unpaired, two-tailed Student's *t*-test. Significance was defined as p values of < 0.05. Statistical analyses were performed using GraphPad Prism version 8.0.

3. Results and discussion

3.1. Preparation and characterization of SAB-loaded liposomes

To study the effect of liposomes composed of different phospholipids on the behavior of SAB *in vivo* after inhalation, we prepared SAB-loaded liposomes by neutral phospholipids (SPC, HSPC, DPPC), anionic phospholipids (DPPG) and cationic phospholipids (DOTAP) *via* an active drug loading method to obtain SPC-Lipo/SAB, HSPC-Lipo/SAB, DPPC-Lipo/SAB, DPPG-Lipo/SAB and DOTAP-Lipo/SAB, respectively (Fig. 2A). The particle size of SAB-loaded liposomes is around 100–200 nm, and the PDI is < 0.3. Except for DOTAP-Lipo/SAB, the surface potentials of all the liposomes are negatively charged (Fig. 2B-C). The LE of SAB is about 70–90%, and the DL is about 5–6% for all the liposomes (Fig. 2D). The morphological appearance of liposomes was observed through TEM (Fig. 2E). SPC-Lipo/SAB, DPPC-Lipo/SAB, DPPG-Lipo/SAB and DOTAP-Lipo/SAB are spherical with fingerprint-like membrane layers, while HSPC-Lipo/SAB is near spherical with a thin film layer. These results showed that liposomes prepared by saturated phospholipids had larger particle sizes, while unsaturated phospholipid and positively charged phospholipid resulted in smaller size. In consistent with previous studies [40,41], the saturation and charges of phospholipids are important factors that determine the particle size and morphology of liposomes.

The release behavior of SAB-loaded liposomes in PBS before and after incubation with artificial mucus (Fig. 2F–G). The cumulative release of SAB from DOTAP-Lipo/SAB is significantly lower than the other groups, and artificial mucus slightly increase the cumulative drug release of DOTAP-Lipo/SAB from 5.87% to 13.20%. It is speculated that the carboxyl group and phenolic hydroxyl group of SAB could combine with the quaternary ammonium salt cationic head group of DOTAP, which hinders drug release [42–44]. Whereas, the electric attractions between SAB and DOTAP might be competitive interfered by mucin. Interestingly, SAB-loaded liposomes constructed by neutral and anionic phospholipids showed similar release behavior in PBS regardless of the presence of artificial mucus, reaching about 50–60% of the total SAB at 12 h. Besides, the stability of SAB-loaded liposomes was monitored in terms of particle size, PDI and zeta potential (Fig. S1A–C), indicating the high stability of all the SAB-loaded liposomes at 4 °C for at least one week.

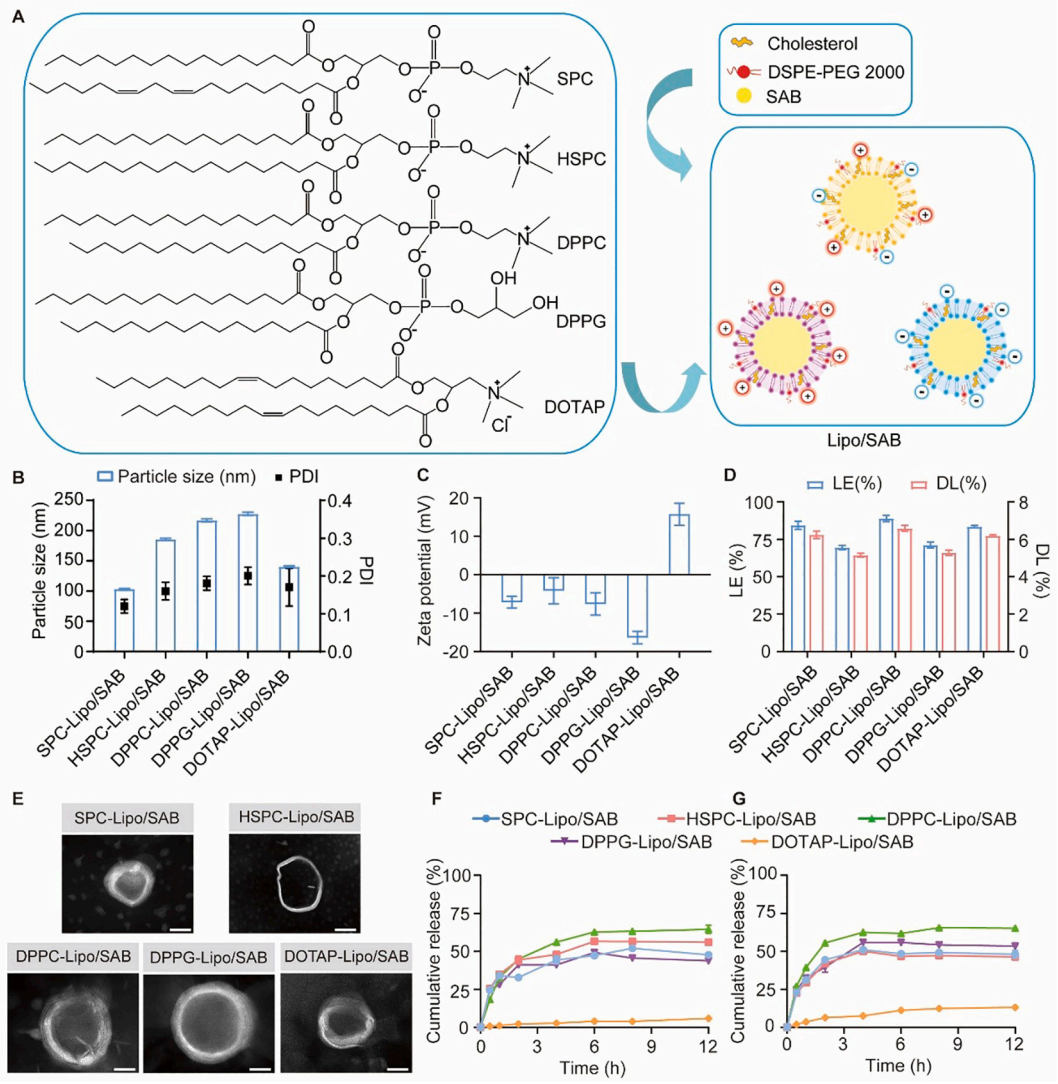

Fig. 2. Characterization of SAB-loaded liposomes composed of different phospholipids. (A) The chemical structure of SPC, HSPC, DPPC, DPPG, and DOTAP and the schematic diagram of liposomes with different surface potential. (B) The particle size, PDI and (C) zeta potential of SAB-loaded liposomes. (D) Drug loading efficiency (LE) and drug loading capacity (DL) of SAB. (E) Representative TEM images of liposomes (scale bar = 50 nm). Release behavior of SAB from liposomes in pH 7.4 PBS (F) without and (G) with artificial mucus added. Each value represents the mean ± SD (n = 3).

3.2. In vitro stability of SAB-loaded liposomes in mucus and BALF

The stability of drug-loaded liposomes in the mucus of pulmonary alveoli is an important factor affecting the penetration and further cellular uptake of SAB. We evaluated the stability of liposomes through the FRET effect and particle size changes in lung-related media. Because the emission spectrum of HIQ can have sufficient overlap with the that of NR, HIQ and NR can be used as a FRET reagent pair (Fig. 3A–B). When HIQ and NR are co-loaded into liposomes, the emission of HIQ can excite NR, which is called FRET effect [45,46]. Whereas the destruction of liposomes leads to the release of HIQ and NR, resulting in the reduction of FRET. We prepared HIQ and NR co-loaded liposomes and characterized (Fig. S2). The emission intensity ratio (I/I_0) at 400/635 nm was detected in mucin, artificial mucus and BALF to evaluate the FRET effects (Fig. 3C–E). In the mucin and artificial mucus, the emission intensity ratio of DOTAP-Lipo/HIQ-NR were reduced, indicating the instability of DOTAP-Lipo/HIQ-NR. Compared with saturated phospholipids, the stability of liposomes composed of SPC in mucin and artificial mucus was slightly reduced, which might be related to the existence of unsaturated bonds in the fatty acid chain. All the liposomes maintained the intact structure in the BALF that might be attributed to the low concentration of pulmonary surfactant proteins.

Moreover, the particle size and PDI of liposomes in mucin solution, artificial mucus and BALF were monitored for 24 h (Fig. 3F–K). The neutral and negative liposomes undergo slight size changes after co-incubating with mucin and artificial mucus, while the electrostatic attractions led to the obvious size increase of DOTAP-Lipo/HIQ-NR. In BALF, the size of DOTAP-Lipo/HIQ-NR slightly increased, while the other liposomal preparations exhibited almost no size increasement. It was contributed to the low concentration of pulmonary surfactant proteins resulting in the weak combination with DOTAP. Besides, all the liposomes exhibited good stability in PBS for 24 h in terms of the emission intensity ratio, diameter and PDI (Fig. S3). Collectively, liposomes composed of neutral and anionic phospholipids maintained high stability in the respiratory tract and pulmonary alveoli after inhalation. Although SPC-Lipo/HIQ-NR exhibited slightly reduced emission intensity ratio in mucin and artificial mucus, small variation on size and PDI was observed. It was suggested that mucin interfered with the stability of SPC-Lipo without breaking the structure integrity of liposomes.

3.3. Interactions between SAB-loaded liposomes and mucin/BALF

Further studies on the interactions between SAB-loaded liposomes and mucin/BALF were evaluated by the physiochemical properties of liposomes and turbidimetry variation. Above all, the size increasement of liposomes at different ratios of mucin to phospholipid (*w/w*) was monitored as well as PDI and zeta potential (Fig. 4A–C). As the amount of mucin increases, the particle size of DOTAP-Lipo/SAB sharply increased. In comparison, size variation was hardly observed in the other liposomes until the mass ratio of mucin to phospholipid reached 2.

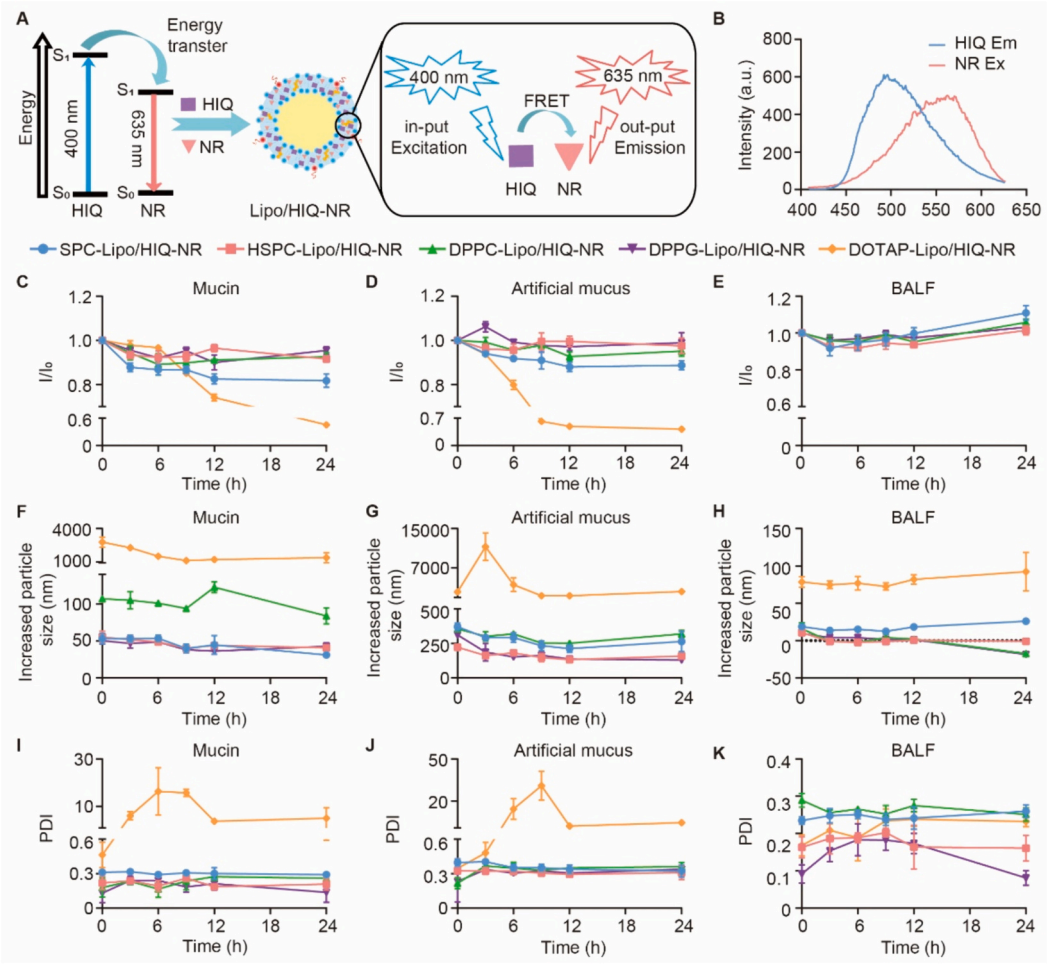

Fig. 3. Stability of HIQ and NR co-loaded liposomes in pulmonary-related media. (A) Illustration of FRET effect between HIQ and NR. (B) Emission spectrum of HIQ and excitation spectrum of the NR. Variation on I/I_0 of HIQ and NR co-loaded liposomes in (C) mucin, (D) artificial mucus and (E) BALF within 24 h. The change of particle size and PDI of HIQ and NR co-loaded liposomes in (F, I) mucin, (G, J) artificial mucus and (*H*, *K*) BALF within 24 h. Each value represents the mean ± SD ($n = 3$).

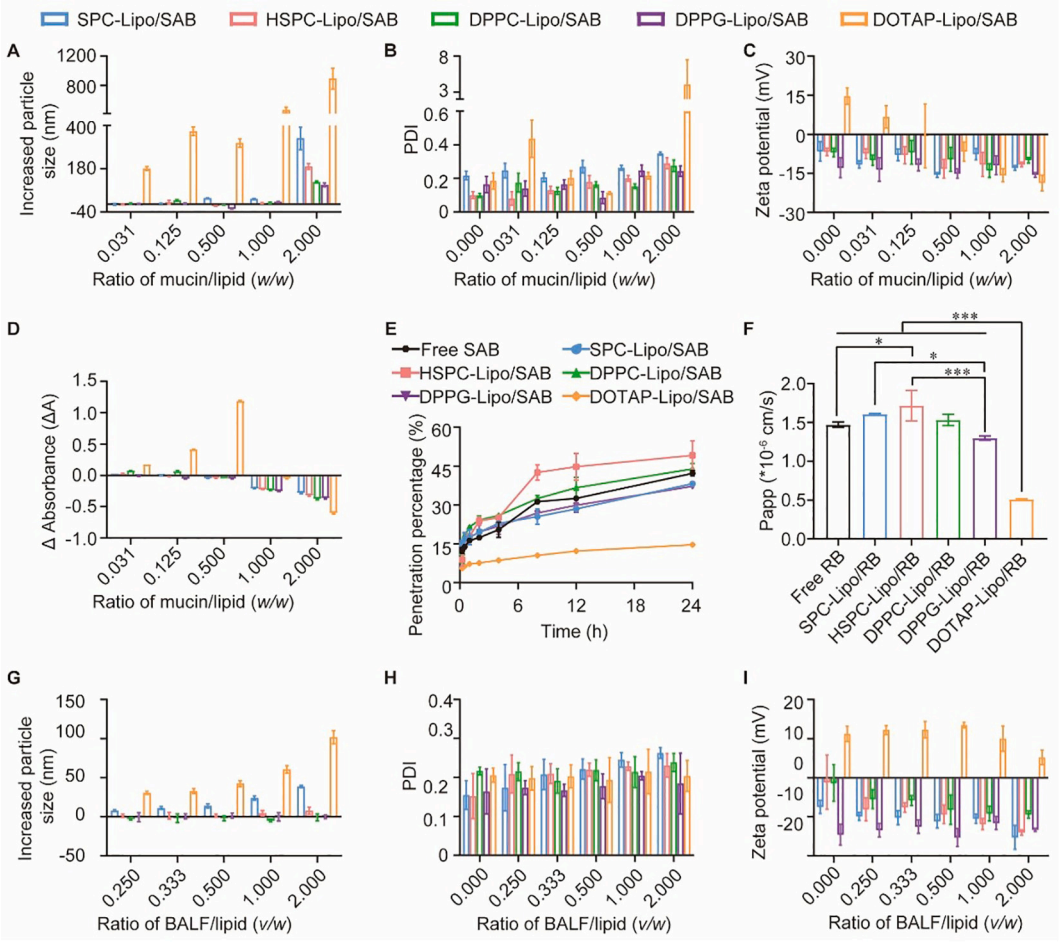

Fig. 4. *In vitro* assessment of the interactions between SAB-loaded liposomes and mucus/BALF. The (A) increased particle size, (B) PDI and (C) zeta potential of mucin-liposome mixtures at different weight ratios of mucin to phospholipids. (D) The absorbance difference (ΔA) between the theoretical absorbance and the actual effective absorbance. (E) The penetration percentage of SAB-loaded liposomes through artificial mucus in transwell and (F) P_{app} at 24 h. (G) The increased particle size, (H) PDI and (I) zeta potential of BALF-liposome mixtures at different ratios of BALF to phospholipids (*v/w*). Each value represents the mean ± SD ($n = 3$), $^{*}p < 0.05$, $^{***}p < 0.001$.

Due to the large number of sialic acid residues on the surface of mucin, it appears to be negative [47,48]. Hence, a charge reversal was observed in DOTAP-Lipo/SAB at the mucin to phospholipid ratio of 0.5 (*w/w*) indicating continuous combination of mucin on the liposomes. However, the zeta potential of SAB-loaded liposomes composed of neutral and anionic phospholipids exhibited slight changes. In addition, we examined the effects of incubation time on the interactions between liposomes and mucin at the mucin to phospholipid ratio of 2.0 (*w/w*) (Fig. S4). The particle size, PDI and zeta potential of DOTAP-Lipo/SAB merely changed after 1 h, which revealed that the interactions between DOTAP-Lipo/SAB and mucin reached the balance quickly. SPC-Lipo/SAB showed sharply increased particle size (>300 nm) at 1 h, while the increased particle size of HSPC-Lipo/SAB was lower than 200 nm even at 48 h. DPPC-Lipo/SAB and DPPG-Lipo/SAB exhibited < 200 nm increased particle size until 24 h. It is speculated that mucin might be involved in the reconstruction of SPC-Lipo/SAB and HSPC-Lipo/SAB effectively prevented the interference from mucin.

Furthermore, the turbidity of liposomes and mucin mixed solution was measured at λ = 500 nm. DOTAP-Lipo/SAB significantly increased the turbidity of mucin, while no obvious change on the absorbance was monitored in the other liposomes (Fig. 4D). Further analysis on the turbidity variation was implemented (Fig. S5). The absorbance of DOTAP-Lipo/SAB increased significantly as the mucin/lipid ratio was <0.125, and the slope of the fitted line was about 5 times of that of the mucin, indicating that DOTAP-Lipo/SAB formed strong interactions with mucin. However, the slope of the fitted line of the other liposomes is even lower than that of the mucin. These results are in agreement with the size variation of liposomes in the mixed solution. The mucus penetration capability of SAB-loaded liposomes was studied *via* a transwell method using the artificial mucus (Fig. 4E–F). DOTAP-Lipo/SAB exhibited the lowest permeability, and the aggregation was clearly observed in the mucus layer (Fig. S6). The other SAB-loaded liposomes possessed similar mucus permeability compared with free SAB. Accumulating evidence indicated that the weak interactions between neutral or negative liposomes and mucin facilitated the mucus penetration [49,50]. While the strong interactions between mucin and DOTAP contributed to the low permeation across mucus layer.

In terms of the interactions between SAB-loaded liposomes and BALF, the size increasement, PDI and zeta potential of liposomes at different ratios of BALF to phospholipid (*v/w*) was monitored (Fig. 4G–I). The particle size of DOTAP-Lipo/SAB increased along with the ratio of BALF/lipid (*v/w*). Meanwhile, the charge of DOTAP-Lipo/SAB reduced, while charge reversal was not observed. Interestingly, the particle size of SPC-Lipo/SAB increased gradually that was different from the size variation in mucin. It was speculated that the size increase of SPC-Lipo/SAB might be attributed to the specific interactions between SPC and pulmonary surfactant proteins.

3.4. Penetration of liposomes across bronchial and alveolar epithelium

HBE135-E6E7 cells and A549 cells were used to establish the bronchial and alveolar epithelial cell monolayer model, respectively. RAW264.7 cells were used to evaluate the alveolar macrophages phagocytosis. Above all, the toxicity of SAB-loaded liposomes on HBE135-E6E7 cells, A549 cells and RAW264.7 cells was determined (Fig. S7–9). The cellular uptake of SAB-loaded liposomes by HBE135-E6E7 cells, A549 cells and RAW264.7 cells after 2 and 4 h of incubation was detected (Fig. 5A–C). DOTAP-Lipo/SAB exhibited the highest cellular uptake by all the cells, which was attributed to the high cell binding ability of the cationic liposomes [51]. HSPC-Lipo/SAB showed higher cellular uptake in A549 cells and RAW264.7 cells at 4 h than the other groups, except for DOTAP-Lipo/SAB. For bronchial and alveolar epithelium penetration study, both HBE135-E6E7 and A549 cell monolayers were established in the upper chamber of transwell. The mucus layer produced by HBE135-E6E7 cells in air-liquid interface for 28 days was identified by alcian blue staining (Fig. S10). Compared with free SAB, DOTAP-Lipo/SAB and HSPC-Lipo/SAB possessed lower P_{app} value in HBE135-E6E7 cell monolayer, especially for DOTAP-Lipo/SAB, while DPPG-Lipo/SAB possessed higher P_{app} value (Fig. 5D). Relative TEER variation of the HBE135-E6E7 cell monolayer after treatments by SAB-loaded liposomes indicated that liposomes opened the tight junctions (Fig. 5E). In terms of A549 cell monolayer, both DPPG-Lipo/SAB and DPPC-Lipo/SAB exhibited much higher P_{app} value than free SAB (Fig. 5F). These results suggested that free SAB may quickly penetrate the cell layer through the cellular pathway and the strong binding force between DOTAP-Lipo/RB and epithelial cells failed to facilitate further transcellular transport.

RB-loaded liposomes with the same formulation and preparation process were prepared and characterized for *in vivo* distribution study (Fig. S11). The fluorescent sections of bronchial tubes and lung tissue at 2 h after inhalation of RB-loaded liposomes (Fig. 5G). Overall fluorescence intensity of free RB was weak due to the quick penetration of RB. HSPC-Lipo/RB showed the strongest fluorescence signal in the slice of lung compared with the other groups, indicating the high retention of HSPC-Lipo/RB in the lung tissue. Focusing on the bronchial tubes, SPC-Lipo/RB possessed the weakest distribution of RB at the bronchial epithelium. It is suggested that saturated phospholipids are more likely to improve the retention of cargos in the lungs. Noteworthy, DOTAP-

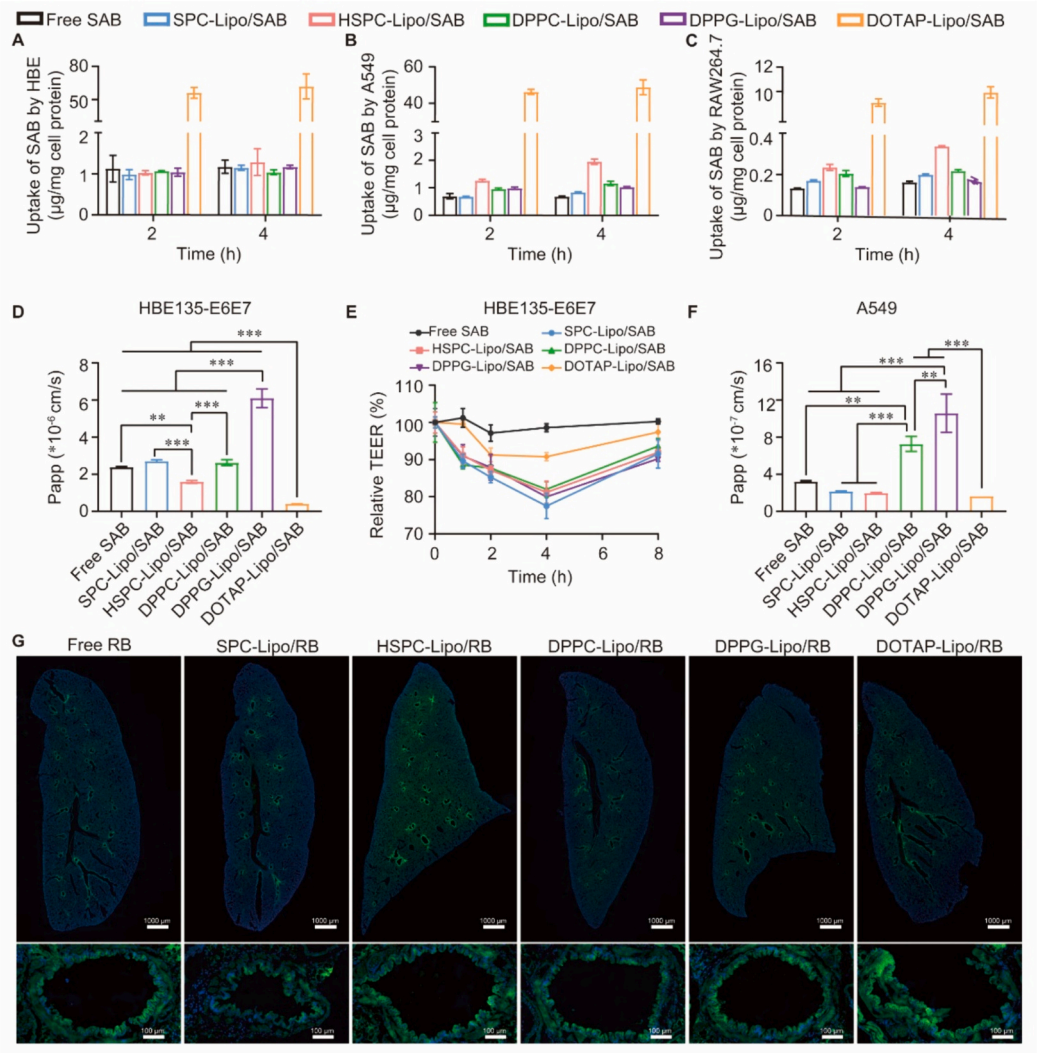

Fig. 5. Liposomes mediate bronchial and alveolar epithelium penetration. Cellular uptake of SAB-loaded liposomes by (A) HBE135-E6E7 cells, (B) A549 cells and (C) RAW264.7 cells after 2 and 4 h of incubation at 37 °C. (D) P_{app} values of SAB-loaded liposomes through the HBE135-E6E7 cell monolayer at 4 h after incubation. (E) Relative TEER of the HBE135-E6E7 cell monolayer after treatments by SAB-loaded liposomes. (F) P_{app} values of SAB-loaded liposomes through the A549 cell monolayer at 4 h after incubation. (G) Distribution of RB-loaded liposomes in the pulmonary and bronchus 2 h post instillation, nucleus was stained by DAPI (blue), RB was green. Each value represents the mean ± SD ($n = 3$), $^{**}p < 0.01$, $^{***}p < 0.001$. (For interpretation of the references to colour in this figure legend, the reader is referred to the web version of this article.)

Lipo/RB accumulated at the bronchial epithelium exhibiting low distribution in pulmonary parenchyma. For liposomes deposited in the respiratory zone, they first encounter the mucus layer, which may change their geometry, surface properties, and thus affect their subsequent *in vivo* fate. The strong interactions between DOTAP-Lipo and mucin might enhance cellular uptake by RAW264.7 cells *via* macrophage phagocytosis. Therefore, both SPC-Lipo and DOTAP-Lipo are not appropriate carriers for drug inhalation.

3.5. *In vivo* biodistribution of liposomes after inhalation

Due to the high cytotoxicity of DOTAP-Lipo/SAB on the HBE135-E6E7 cells, A549 cells and RAW264.7 cells, and the lower mucus layer permeability compared with the other SAB-loaded liposomes, as well as the high hemolysis activity (Fig. S12), DOTAP-Lipo/SAB was not involved in the following *in vivo* studies. HSPC-Lipo/SAB, DPPC-Lipo/SAB and DPPG-Lipo/SAB with high mucus stability and mucus layer permeability were applied in the biodistribution and IPF treatments studies. To observe the spatiotemporal distribution of liposomes after inhalation, we prepared DiR-labeled liposomes (Fig. S13). The biodistribution of DiR-labeled liposomes at different time points after tracheal instillation was captured by IVIS (Fig. 6A). Free DiR appeared systemic distribution. However, DiR-labeled liposomes showed smaller range of biodistribution. The pictures of all the organs at 24 h clearly showed the higher fluorescence intensity of DiR at lung in the liposome groups, but there was no statistical difference in the quantitative analysis of fluorescence among DiR-labeled liposomes (Fig. 6B–C). It is suggested that liposomes have the potential to be remained at lung, while the IVIS cannot show the detailed spatiotemporal distribution of SAB-loaded liposomes at lung tissue, which is of great significance for the treatment of pulmonary fibrosis.

To obtained more detailed information about the distribution of SAB at lung, we monitored the SAB content in BALF and the lavaged lung. Moreover, we divided BALF into supernatant and sediment. According to the previous studies, the alveolar macrophages account for 95% of the total number of cells in BALF [52], thereby the drug in BALF sediment can be considered as the NPs that being taken up by alveolar macrophages and not yet been cleared [53]. The SAB content in the lavaged lung represents the amount of SAB accumulated in the lung parenchyma, while the content of SAB in the whole lung contained the SAB in BALF and lavaged lung. The drug concentration-time curve of SAB in BALF supernatant and sediment, whole BALF, lavaged lung and whole lung, as well as plasma were plotted (Fig. 7A–F). Correspondingly, the pharmacokinetic parameters were calculated (Fig. 7G). The results showed that the $AUC_{0\text{-}t}$ of SAB in the BALF supernatant of the HSPC-Lipo/SAB, DPPC-Lipo/SAB and DPPG-Lipo/SAB groups were 2.40, 2.33 and 1.66 times higher than those of the free SAB group, respectively. Although liposomes significantly increased the $AUC_{0\text{-}t}$ of SAB in the BALF sediment, the proportion of SAB is < 1.6% of total dose. In general, liposomes increased the total retention of SAB in BALF. Compared with the free SAB, liposomes increased the absorption of SAB in the lung parenchyma. The $AUC_{0\text{-}t}$ values of the HSPC-Lipo/SAB,

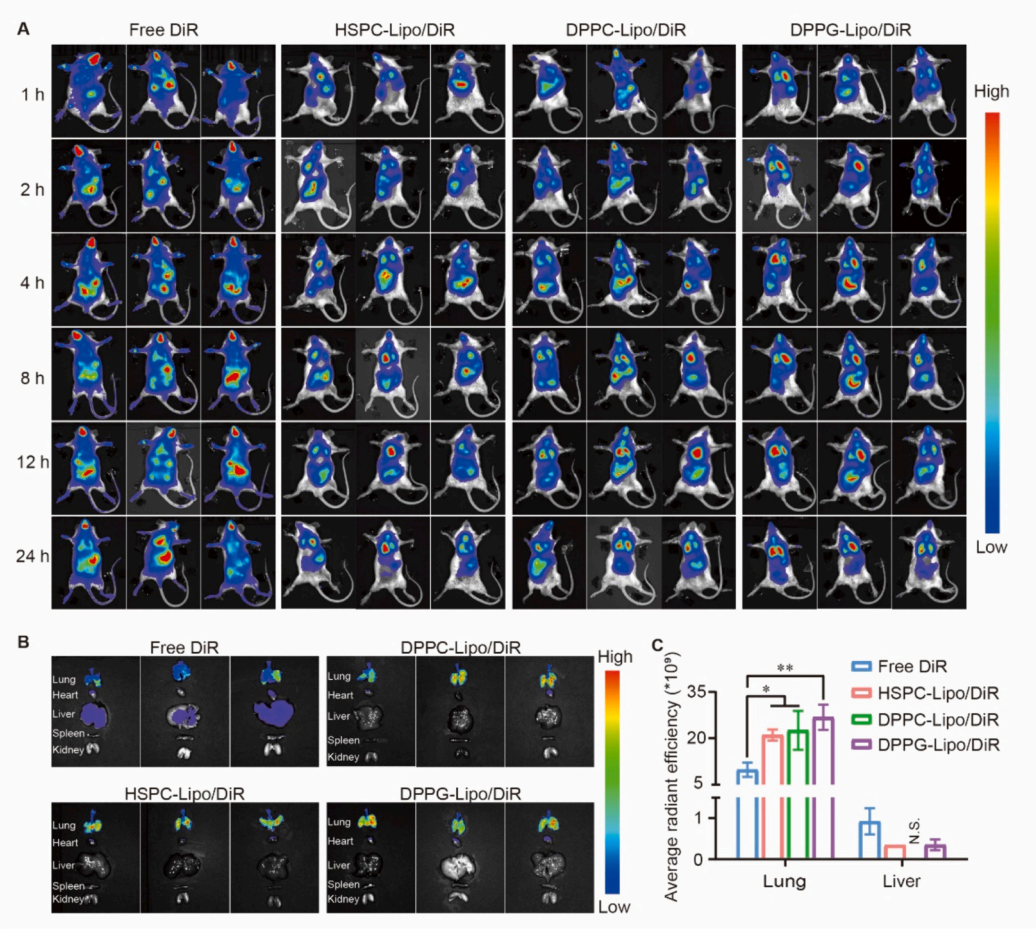

Fig. 6. Biodistribution of DiR-labeled liposomes composed of different phospholipids after intratracheal administration. (A) The *in vivo* near-infrared fluorescence images of mice captured at 1, 2, 4, 8, 12 and 24 h after intratracheal administration by an *in vivo* imaging system. (B) *Ex vivo* imaging of transplanted lung, heart, liver, spleen, and kidney of the mice at 24 h. (C) Quantitation of radiant efficiency in lung and liver of mice. Each value represents the mean ± SD ($n = 3$), $^{*}p < 0.05$, $^{**}p < 0.01$.

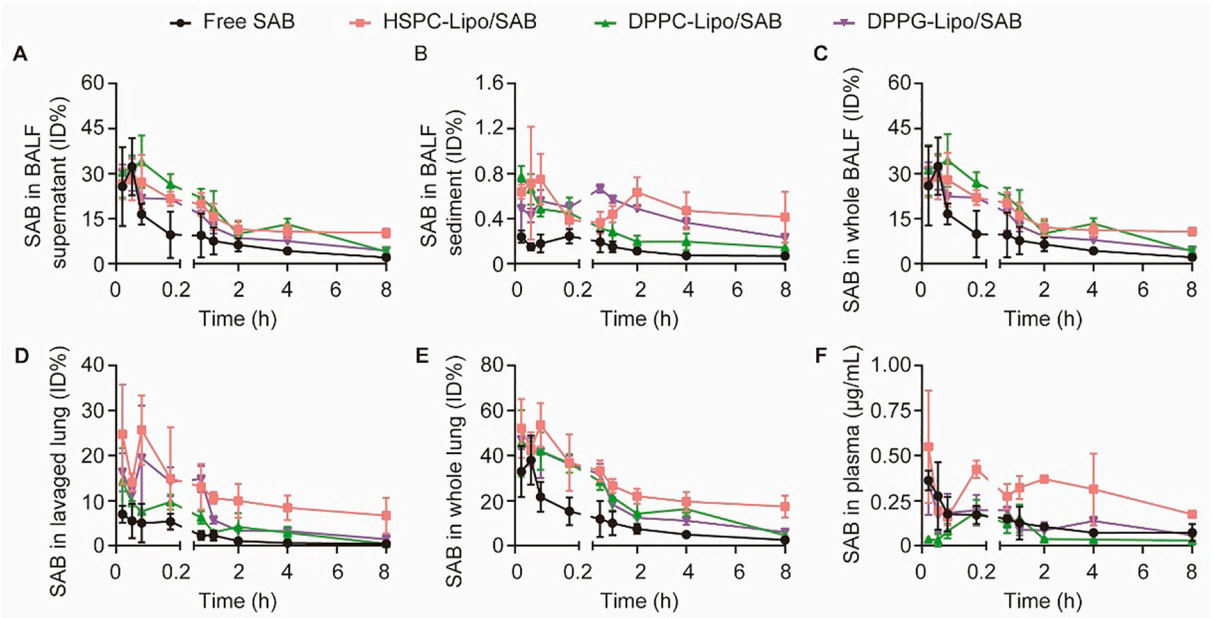

G Pharmacokinetic parameters of SAB retention percentages in the BALF supernatant, BALF sediment, whole BALF, lavaged lung, whole lung, and pharmacokinetic parameters of SAB concentration in the plasma. (means ± SD, n = 3)

	Formulations	$AUC_{0\text{-}t}$ (ID%·h) or (μg/mL·h)	$MRT_{0\text{-}t}$ (h)	T_{max} (h)	C_{max} (ID%) or (μg/mL)
BALF supernatant	Free SAB	40.43 ± 4.34	2.75 ± 0.30	0.04 ± 0.01	36.01 ± 7.79
	HSPC-Lipo/SAB	97.14 ± 5.07 ***	3.54 ± 0.11 *	0.06 ± 0.01	31.80 ± 1.19
	DPPC-Lipo/SAB	94.39 ± 14.84 **	2.86 ± 0.11 #	0.05 ± 0.02	37.68 ± 2.98
	DPPG-Lipo/SAB	67.21 ± 4.92 #	2.95 ± 0.11 #	0.03 ± 0.01	31.36 ± 3.67
BALF sediment	Free SAB	0.79 ± 0.04	3.14 ± 0.20	0.23 ± 0.20	0.29 ± 0.02
	HSPC-Lipo/SAB	3.84 ± 0.55 ***	3.76 ± 0.32	0.69 ± 0.93	0.89 ± 0.29 *
	DPPC-Lipo/SAB	1.67 ± 0.22 ###	3.29 ± 0.11	0.03 ± 0.01	0.81 ± 0.05 *
	DPPG-Lipo/SAB	3.16 ± 0.15 *** $$	3.20 ± 0.06	0.34 ± 0.23	0.69 ± 0.06
Whole BALF	Free SAB	41.13 ± 4.36	2.76 ± 0.30	0.04 ± 0.01	36.20 ± 7.83
	HSPC-Lipo/SAB	100.97 ± 5.17 ***	3.55 ± 0.11 **	0.06 ± 0.01	32.56 ± 1.54
	DPPC-Lipo/SAB	96.06 ± 14.94 ***	2.87 ± 0.10 #	0.05 ± 0.02	38.34 ± 2.92
	DPPG-Lipo/SAB	70.37 ± 5.07 * #	2.96 ± 0.11 #	0.03 ± 0.01	31.73 ± 3.70
Lavaged lung	Free SAB	8.55 ± 0.47	2.25 ± 0.33	0.04 ± 0.03	8.20 ± 0.89
	HSPC-Lipo/SAB	72.61 ± 6.19 ***	3.47 ± 0.45 *	0.06 ± 0.03	30.66 ± 0.95 **
	DPPC-Lipo/SAB	23.59 ± 7.31 ##	2.40 ± 0.19 #	0.07 ± 0.07	14.91 ± 5.59 #
	DPPG-Lipo/SAB	32.87 ± 2.51 ** ###	2.42 ± 0.17 #	0.25 ± 0.18	22.35 ± 7.01
Whole lung	Free SAB	49.77 ± 4.05	2.67 ± 0.24	0.03 ± 0.01	41.72 ± 7.30
	HSPC-Lipo/SAB	173.58 ± 6.13 ***	3.50 ± 0.21 **	0.05 ± 0.02	55.52 ± 7.22
	DPPC-Lipo/SAB	119.65 ± 22.24 ** ##	2.78 ± 0.11 #	0.05 ± 0.02	51.48 ± 7.05
	DPPG-Lipo/SAB	103.24 ± 6.93 * ##	2.79 ± 0.09 #	0.05 ± 0.02	48.49 ± 4.67
Plasma	Free SAB	0.73 ± 0.11	3.32 ± 0.48	0.03 ± 0.01	0.37 ± 0.04
	HSPC-Lipo/SAB	2.32 ± 0.55 **	3.43 ± 0.07	0.12 ± 0.07	0.58 ± 0.24
	DPPC-Lipo/SAB	0.42 ± 0.00 ###	2.66 ± 0.59	0.72 ± 0.39	0.22 ± 0.04
	DPPG-Lipo/SAB	0.87 ± 0.08 ##	3.38 ± 0.14	0.19 ± 0.22	0.37 ± 0.14

Fig. 7. Retention of SAB in the lung and circulation of normal mice after intratracheal administration. The retention percentages-time profiles of SAB in (A) BALF supernatant, (B) BALF sediment, (C) whole BALF, (D) lavaged lung, (E) whole lung, and (F) plasma. (G) Pharmacokinetic parameters of SAB in the BALF supernatant, BALF sediment, whole BALF, lavaged lung, whole lung, and the plasma. Each value represents the mean ± SD ($n = 3$), $^{*}p < 0.05$, $^{**}p < 0.01$, $^{***}p < 0.001$ compared with free SAB group, $^{\#}p < 0.05$, $^{\#\#}p < 0.01$, $^{\#\#\#}p < 0.001$ compared with HSPC-Lipo/SAB group, $^{\$\$}p < 0.01$ compared with DPPG-Lipo/SAB group.

DPPC-Lipo/SAB and DPPG-Lipo/SAB groups were 8.49, 2.76 and 3.84 times higher than those of the free SAB group, respectively. A significant increase in the retention of SAB was observed in the whole lung. Interestingly, no absorption peak was observed on the plasma drug concentration-time curve of free SAB in comparison with liposomes, indicating quick systemic escape of SAB after inhalation. The $AUC_{0\text{-}t}$ of HSPC-Lipo/SAB, DPPC-Lipo/SAB and DPPG-Lipo/SAB groups in plasma were 3.18, 0.58 and 1.19 times higher than that of free SAB group, respectively. It is speculated that the retention of liposomes in BALF results in the prolonged absorption phase. Besides, the distribution of SAB in heart, liver, spleen, and kidney tissues over time were measured as well (Fig. S14).

When nanoparticles pass through the upper respiratory tract, they are liable to be eliminated by mucociliary movement, thereby reducing lung deposition. PEGylation can effectively reduce mucociliary clearance of liposomes and facilitate the mucus layer penetration. However, the phospholipids used for the construction of liposomes can significantly affect *in vivo* fate of liposomes *via* the size, structure, and surface

charge. HSPC, DPPC and DPPG based liposomes enhanced the retention of SAB in BALF supernatant, thereby improving the absorption of SAB by pulmonary parenchyma. Since DPPC and DPPG are important components of endogenous pulmonary surfactant and endogenous substances for the formation of lipid-protein conjugates (such as tubular myelin located in the lung alveoli), they have good biocompatibility and can effectively improve the retention of SAB in the lungs [54–56]. In addition, DPPG as a fusogenic lipid can regulate membrane fluidity and improve cellular uptake by promoting the fusion of liposomes with cell membranes [57,58]. In terms of HSPC, the high phase transition temperature endowed HSPC-Lipo/SAB high stability, leading to prolonged residence time of SAB in BALF, pulmonary parenchyma and systemic circulation [59,60]. It is worth noting that although the cellular uptake of liposomes by alveolar macrophages was significantly increased, it accounted for a low proportion of the total dose. Collectively, liposomes prolong the lung exposure time of SAB mainly through BALF retention rather than macrophage phagocytosis.

3.6. Therapeutic effects of SAB-loaded liposomes on IPF

Liposomes composed of HSPC, DPPC and DPPG enhanced the residence time of SAB in the lungs after inhalation, which is in favor of the treatment for lung diseases. We explored the anti-fibrotic effect of HSPC-Lipo/SAB, DPPC-Lipo/SAB and DPPG-Lipo/SAB on the BLM-induced IPF mice. BLM, a glycoside antibiotic, can cause lung inflammation and fibrosis in the short term. The histological changes in the BLM-induced

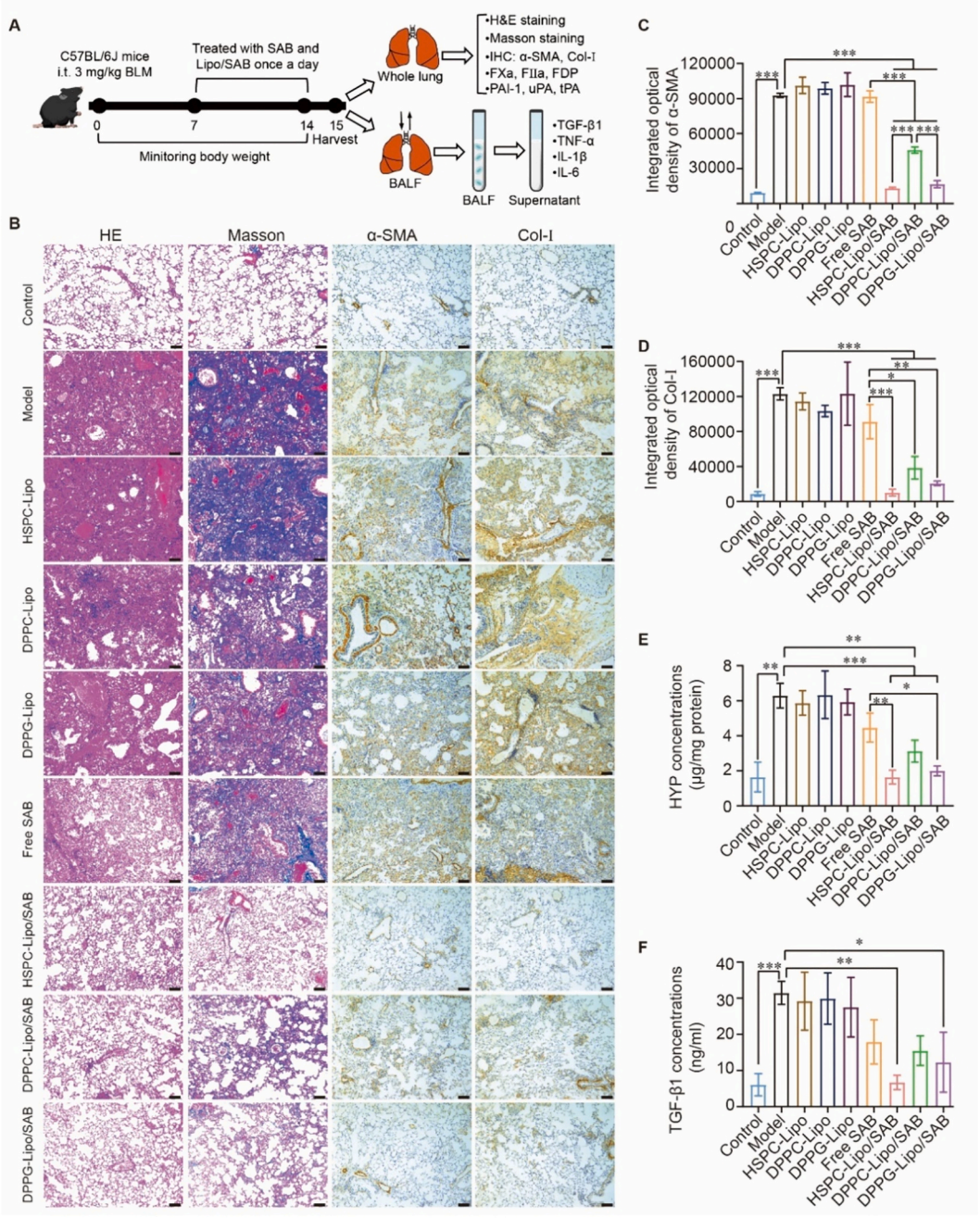

Fig. 8. Therapeutic effect of SAB-loaded liposomes on BLM-induced IPF mice. (A) Schematic illustration for the evaluation of SAB-loaded liposomes on IPF mice. (B) Representative histologic analyses of lung sections, including H&E staining, Masson's staining and immunohistochemical staining of α-SMA and Col-I (scale bar = 50 μm). The integrated optical density of (C) α-SMA and (D) Col-I were analyzed with Image J. Quantitation of the protein level of (E) HYP by HYP kit and (F) TGF-β1 by TGF-β1 ELISA kit. Each value represents the mean ± SD ($n = 3$), *$p < 0.05$, **$p < 0.01$, ***$p < 0.001$.

IPF mice model can reflect the pathological characteristics of IPF in patients [15,61]. In this study, one-dose of BLM (3 mg/kg) injected *via* tracheal intubation was used to establish IPF mice model. SAB were injected after 7 days *via* tracheal intubation at a dose of 5 mg/kg, once a day for one week, and the mice were anesthetized at the 15th day (Fig. 8A). During this period, the weight and activity status of mice were recorded, and the lung coefficients of the mice were calculated at the end point of study for preliminary evaluation of the therapeutic effects (Fig. S15). The mice in the control group were in good condition, with stable breathing, agile movements, good diet, shiny fur, and slight weight gain. After BLM inhalation, the mice in the model group experienced rapid breathing, slow movement, significant reduction in food intake and drinking water, fried hair, and sharp weight loss. After treatments by SAB-loaded liposomes, the symptoms of IPF in mice was partly alleviated indicating by the stable breath and less weight loss.

H&E and Masson's staining were used to evaluate the histopathological changes in the lungs of mice (Fig. 8B). Compared with the lungs of normal mice, the lungs of mice in the model group showed obvious abnormal morphological changes, including collapse of alveolar cavity, loss of alveolar structure, thickening of alveolar/bronchial walls, and infiltration of inflammatory cells. After the treatments by SAB-loaded liposomes, we observed a significant amelioration on lung injury, which was evaluated by the inflammation and tissue damage scoring system (Fig. S16A). Masson's staining further confirmed the anti-fibrotic effect of SAB-loaded liposomes. A large area of muscle fibers was observed in the lungs of mice in the model group, and a large number of proliferated blue collagen fibers appeared around blood vessels and bronchi. Compared with the mice in model group, SAB-loaded liposomes treated mice possessed reduced collagen fiber and pulmonary interstitial fibrosis (Fig. S16B). Alpha-SMA and Col-I were quantified to further estimate the pulmonary fibrosis in mice (Fig. 8C–D). Compared with the control group, the expression of α-SMA and Col-I significantly increased in the model group. After treatments by SAB preparations, the expression of α-SMA and Col-I in the lung decreased obviously. As evidenced by the level of HYP in the lung (Fig. 8E) and the level of TGF-β1 in the BALF (Fig. 8F), SAB-loaded liposomes were confirmed with improved therapeutic effects on the IPF in comparison to free SAB. HSPC-Lipo/SAB and DPPG-Lipo/SAB exhibited better anti-fibrosis effects than DPPC-Lipo/SAB with no significant differences.

Free SAB have been verified with effective inhibitory effects on pulmonary fibrosis *via* inhalation as solution [14] or dry powder [13,15]. However, the high aqueous solubility of SAB might result in less cellular uptake by pulmonary alveolar cells, as well as short retention in the lung and circulation that was confirmed by the pharmacokinetics study in this work. Although liposomes could improve the retention of SAB in the BALF and lung, the airway pili-phlegm clearance became new problems for liposomes. Hence, systemic evaluation of liposomes regarding to the permeability across mucus layer and epithelium as well as the lung retention capability are necessary. According to the *in vitro* and *in vivo* evaluation, the superior anti-fibrotic effect of DPPG-Lipo/

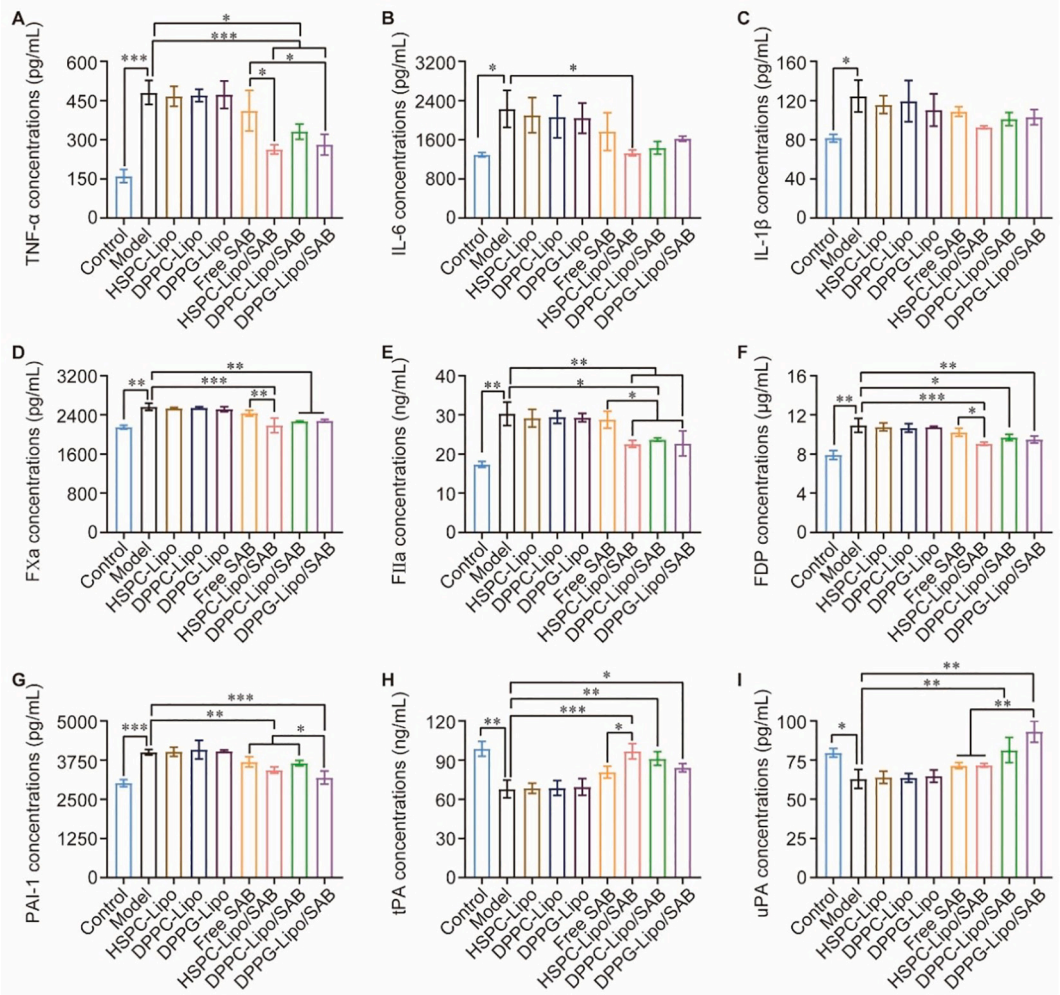

Fig. 9. Effects on inflammatory factors and coagulation-fibrinolysis system in IPF mice. Quantitation of the protein levels of inflammatory factor (A) TNF-α, (B) IL-6 and (C) IL-1β in BALF, and protein levels of coagulation-fibrinolysis system related factors (D) FXa, (E) FIIa, (F) FDP, (G) PAI-1, (H) tPA and (I) uPA. Each value represents the mean ± SD ($n = 3$), $^{*}p < 0.05$, $^{**}p < 0.01$, $^{***}p < 0.001$.

SAB might be closely related to their high permeability across bronchial and alveolar epithelium resulting in long retention at the lung. In terms of HSPC-Lipo/SAB, the better anti-fibrotic effect might be attributed to their high permeability and stability in mucus layer and long retention in the lung and circulation.

We further explored the anti-fibrotic mechanisms of SAB *in vivo via* measuring the expression levels of inflammatory factors and coagulation-plasminogen-related factors in BALF and lung tissue (Fig. 9). After inhalation of SAB-loaded liposomes, the levels of TNF-α, IL-6 and IL-1β in the BALF supernatant of IPF mice decreased (Fig. 9A–C), indicating that the anti-pulmonary fibrosis effect of SAB is related to its inhibitory effects on inflammatory response. Previous studies have shown that the anti-pulmonary fibrosis effect of SAB may be related to its intervention on the coagulation-fibrinolytic system [14]. Therefore, we measured the levels of coagulation factors and plasminogen-related factors in lung tissue after SAB treatment (Fig. 9D–I). The results showed that SAB-loaded liposomes significantly reduced the secretion levels of FXa, FIIa, FDP and PAI-1 in lung tissue, while up-regulated the expressions of uPA and tPA. Intriguingly, HSPC-Lipo/SAB, DPPC-Lipo/SAB and DPPG-Lipo/SAB groups exhibited similar effects on the inflammation inhibition and coagulation-fibrinolytic system regulation. It is hypothesized that the variation of cytokines might be not obvious in a short period and a long-term model establishment might exaggerate the fluctuation of key protein levels.

4. Conclusions

In this study, we establish a systemic *in vitro* and *in vivo* evaluation method to estimate the pulmonary delivery efficiency of SAB *via* inhalation after loaded in the liposomes. We found that the different phospholipids composition of liposomes affected their *in vivo* fate after inhalation, thereby affecting the therapeutic effect of SAB on IPF. It was confirmed that neutral or anionic phospholipids with saturated fat chains are more eligible for the construction of inhalable liposomes, which endowed the high exposure and long-term retention of SAB and improved the therapeutic effects on IPF.

CRediT authorship contribution statement

Jianqing Peng: Writing – review & editing, Writing – original draft, Investigation, Data curation, Conceptualization. **Qin Wang:** Writing – original draft, Methodology, Investigation, Data curation, Conceptualization. **Runbin Sun:** Validation, Formal analysis, Data curation. **Ke Zhang:** Formal analysis, Data curation. **Yi Chen:** Writing – review & editing, Resources, Project administration, Funding acquisition. **Zipeng Gong:** Writing – review & editing, Supervision, Project administration, Funding acquisition.

Declaration of competing interest

The authors declare that the research was conducted in the absence of any commercial or financial relationships that could be construed as a potential conflict of interest.

Data availability

Data will be made available on request.

Acknowledgements

This work was supported by the National Natural Science Foundation of China (82104537, 82360780), High-level Overseas Talent Fund for Home Work From Ministry of Human Resources and Social Security (No. RSBLXHGZ202001), Natural Science Research Foundation of Guizhou Provincial Department of Education (qianjiaoji066), the Excellent Young Talents Plan of Guizhou [QKHPTRC-YQK[2023]029], the Excellent Young Talents Plan of Guizhou Medical University (2020-102, 2021-103, 2022-104), Chinese Society of Traditional Chinese Medicine youth talent lifting project [CACM-(2023-QNRC2-B14)].

Appendix A. Supplementary data

Supplementary data to this article can be found online at https://doi.org/10.1016/j.jconrel.2024.05.026.

References

[1] T.M. Maher, E. Bendstrup, L. Dron, J. Langley, G. Smith, J.M. Khalid, H. Patel, M. Kreuter, Global incidence and prevalence of idiopathic pulmonary fibrosis, Respir. Res. 22 (1) (2021) 197, https://doi.org/10.1186/s12931-021-01791-z.
[2] T. Zhao, B.K. Gong, S.Q. Luo, R.P. Zhang, L. Zhang, Y. Huang, H.L. Gao, T. Gong, A fibroblastic foci-targeting and hypoxia-cleavable delivery system of pirfenidone for the treatment of idiopathic pulmonary fibrosis, Acta Biomater. 167 (2023) 574–582, https://doi.org/10.1016/j.actbio.2023.06.024.
[3] D.S. Glass, D. Grossfeld, H.A. Renna, P. Agarwala, P. Spiegler, J. DeLeon, A. B. Reiss, Idiopathic pulmonary fibrosis: current and future treatment, Clin. Respir. J. 16 (2) (2022) 84–96, https://doi.org/10.1111/crj.13466.
[4] G. Raghu, H.R. Collard, J.J. Egan, F.J. Martinez, J. Behr, K.K. Brown, T.V. Colby, J.-F. Cordier, K.R. Flaherty, J.A. Lasky, D.A. Lynch, J.H. Ryu, J.J. Swigris, A.U. Wells, J. Ancochea, D. Bouros, C. Carvalho, U. Costabel, M. Ebina, D.M. Hansell, T. Johkoh, D.S. Kim, T.E. King, Y.K. Jr, J. Myers, Nestor L. Müller, A.G. Nicholson, L. Richeldi, M. Selman, R.F. Dudden, B.S. Griss, S.L. Protzko, H.J. Schünemann, An official ATS/ERS/JRS/ALAT statement: idiopathic pulmonary fibrosis: evidence-based guidelines for diagnosis and management, Am. J. Respir. Crit. Care Med. 183 (6) (2011) 788–824, https://doi.org/10.1164/rccm.2009-040GL.
[5] L. Richeldi, H.R. Collard, M.G. Jones, Idiopathic pulmonary fibrosis, Lancet 389 (10082) (2017) 1941–1952, https://doi.org/10.1016/s0140-6736(17)30866-8.
[6] B.J. Moss, S.W. Ryter, I.O. Rosas, Pathogenic mechanisms underlying idiopathic pulmonary fibrosis, Annu. Rev. Pathol. 17 (2022) 515–546, https://doi.org/10.1146/annurev-pathol-042320-030240.
[7] P. Spagnolo, J.A. Kropski, M.G. Jones, J.S. Lee, G. Rossi, T. Karampitsakos, T. M. Maher, A. Tzouvelekis, C.J. Ryerso, Idiopathic pulmonary fibrosis: disease mechanisms and drug development, Pharmacol. Ther. 222 (2021) 107798, https://doi.org/10.1016/j.pharmthera.2020.107798.
[8] V. Navaratnam, A.W. Fogarty, T. McKeever, N. Thompson, G. Jenkins, S. R. Johnson, G. Dolan, M. Kumaran, K. Pointon, R.B. Hubbard, Presence of a prothrombotic state in people with idiopathic pulmonary fibrosis: a population-based case-control study, Thorax 69 (3) (2014) 207–215, https://doi.org/10.1136/thoraxjnl-2013-203740.
[9] E. Bargagli, C. Madioni, N. Bianchi, R.M. Refini, R. Cappelli, P. Rottoli, Serum analysis of coagulation factors in IPF and NSIP, Inflammation 37 (1) (2014) 10–16, https://doi.org/10.1007/s10753-013-9706-z.
[10] I. Kotani, A. Sato, H. Hayakawa, T. Urano, Y. Takada, A. Takada, Increased procoagulant and antifibrinolytic activities in the lungs with idiopathic pulmonary fibrosis, Thromb. Res. 77 (6) (1995) 493–504, https://doi.org/10.1016/0049-3848(95)00025-9.
[11] M. Wygrecka, G. Kwapiszewska, E. Jablonska, S.V. Gerlach, I. Henneke, D. Zakrzewicz, A. Guenther, K.T. Preissner, P. Markart, Role of protease-activated receptor-2 in idiopathic pulmonary fibrosis, Am. J. Respir. Crit. Care Med. 183 (12) (2011) 1703–1714, https://doi.org/10.1164/rccm.201009-1479OC.
[12] X.D. Meim, Y.F. Cao, Y.Y. Che, J. Li, Z.P. Shang, W.J. Zhao, Y.J. Qiao, J.Y. Zhang, Danshen: a phytochemical and pharmacological overview, Chin. J. Nat. Med. 17 (1) (2019) 59–80, https://doi.org/10.1016/s1875-5364(19)30010-x.
[13] L.X. Jiang, Y.J. Li, J.Q. Yu, J.H. Wang, J.R. Ju, J.D. Dai, A dry powder inhalable formulation of salvianolic acids for the treatment of pulmonary fibrosis: safety, lung deposition, and pharmacokinetic study, Drug Deliv. Transl. Res. 11 (5) (2021) 1958–1968, https://doi.org/10.1007/s13346-020-00857-7.
[14] T.Y. Zhang, M.J. Liu, Y.H. Gao, H. Li, L. Song, H.P. Hou, T.F. Chen, L.N. Ma, G. P. Zhang, Z.G. Ye, Salvianolic acid B inhalation solution enhances antifibrotic and anticoagulant effects in a rat model of pulmonary fibrosis, Biomed. Pharmacother. 138 (2021) 111475, https://doi.org/10.1016/j.biopha.2021.111475.
[15] P. Lu, J.W. Li, C.X. Liu, J. Yang, H. Peng, Z.F. Xue, Z.D. Liu, Salvianolic acid B dry powder inhaler for the treatment of idiopathic pulmonary fibrosis, Asian J. Pharm. Sci. 17 (3) (2022) 447–461, https://doi.org/10.1016/j.ajps.2022.04.004.
[16] C.S. Shi, H.C. Huang, H.L. Wu, C.H. Kuo, B. Chang, M.S. Shiao, G.Y. Shi, Salvianolic acid B modulates hemostasis properties of human umbilical vein endothelial cells, Thromb. Res. 119 (6) (2007) 769–775, https://doi.org/10.1016/j.thromres.2006.06.008.
[17] S.Q. He, J.J. Gui, K. Xiong, M.W. Chen, H.L. Gao, Y. Fu, A roadmap to pulmonary delivery strategies for the treatment of infectious lung diseases, J. Nanobiotechnol. 20 (1) (2022) 101, https://doi.org/10.1186/s12951-022-01307-x.
[18] W.H. Wang, Z.W. Huang, Y. Huang, X.J. Zhang, J.Y. Huang, Y.T. Cui, X. Yue, C. Ma, F.Q. Fu, W.H. Wang, C.B. Wu, X. Pan, Pulmonary delivery nanomedicines towards circumventing physiological barriers: strategies and characterization approaches, Adv. Drug Deliv. Rev. 185 (2022) 114309, https://doi.org/10.1016/j.addr.2022.114309.
[19] Q.Y. Liu, J. Guan, L. Qin, X. Zhang, S.R. Mao, Physicochemical properties affecting the fate of nanoparticles in pulmonary drug delivery, Drug Discov. Today 25 (1) (2020) 150–159, https://doi.org/10.1016/j.drudis.2019.09.023.

[20] Y. Guo, H. Bera, C.Z. Shi, L. Zhang, D.M. Cun, M.S. Yang, Pharmaceutical strategies to extend pulmonary exposure of inhaled medicines, Acta Pharm. Sin. B 11 (8) (2021) 2565–2584, https://doi.org/10.1016/j.apsb.2021.05.015.
[21] J.P. Wong, H.M. Yang, K.L. Blasetti, G. Schnell, J. Conley, L.N. Schofield, Liposome delivery of ciprofloxacin against intracellular Francisella tularensis infection, J. Control. Release 92 (3) (2003) 265–273, https://doi.org/10.1016/s0168-3659(03)00358-4.
[22] K. Nahar, J. Rashid, S. Absar, F.I. Al-Saikhan, F. Ahsan, Liposomal aerosols of nitric oxide (NO) donor as a long-acting substitute for the ultra-short-acting inhaled NO in the treatment of PAH, Pharmacol. Res. 33 (7) (2016) 1696–1710, https://doi.org/10.1007/s11095-016-1911-7.
[23] M. Bassetti, A. Vena, A. Russo, M. Peghin, Inhaled liposomal antimicrobial delivery in lung infections, Drugs 80 (13) (2020) 1309–1318, https://doi.org/10.1007/s40265-020-01359-z.
[24] J. Zhao, L. Qin, R.X. Song, J. Su, Y. Yuan, X. Zhang, S.R. Mao, Elucidating inhaled liposome surface charge on its interaction with biological barriers in the lung, Eur. J. Pharm. Biopharm. 172 (2022) 101–111, https://doi.org/10.1016/j.ejpb.2022.01.009.
[25] J. Weers, Comparison of phospholipid-based particles for sustained release of ciprofloxacin following pulmonary administration to bronchiectasis patients, Pulmonary Therapy 5 (2) (2019) 127–150, https://doi.org/10.1007/s41030-019-00104-6.
[26] G. Sheng, N. Tian, H.J. Duan, A.G. Sun, H.Q. Chu, Advances in therapeutic nanodrug delivery systems for infectious lung diseases: a review, Acta Materia Medica 1 (3) (2022) 343–364, https://doi.org/10.15212/amm-2022-0019.
[27] A.M. Shen, T. Minko, Pharmacokinetics of inhaled nanotherapeutics for pulmonary delivery, J. Control. Release 326 (2020) 222–244, https://doi.org/10.1016/j.jconrel.2020.07.011.
[28] F. Rommasi, N. Esfandiari, Liposomal nanomedicine: applications for drug delivery in cancer therapy, Nanoscale Res. Lett. 16 (1) (2021) 95, https://doi.org/10.1186/s11671-021-03553-8.
[29] M.S. Han, Y.J. Song, S. Liu, X.Y. Lu, L.Y. Su, M.X. Liu, X.S. Zhu, K.X. Sun, Y.A. Lu, A.P. Wang, Engineering of stimulus-responsive pirfenidone liposomes for pulmonary delivery during treatment of idiopathic pulmonary fibrosis, Front. Pharmacol. 13 (2022) 882678, https://doi.org/10.3389/fphar.2022.882678.
[30] Z.M. Cai, Q. Wang, J.Z. Xu, J. Zhou, Z.H. Jiang, D. Pan, Y.Y. Zhang, L. Tao, J. Q. Peng, Y. Chen, X.C. Shen, Enhanced protective activity of 1,8-cineole on emphysema using hyaluronic acid-coated liposomes via quantitative pulmonary administration in mice, J. Drug Deliv. Sci. Technol. 72 (2022) 103402, https://doi.org/10.1016/j.jddst.2022.103402.
[31] J.Q. Peng, Z.M. Cai, Q. Wang, J. Zhou, J.Z. Xu, D. Pan, T.T. Chen, G.Q. Zhang, L. Tao, Y. Chen, X.C. Shen, Carboxymethyl chitosan modified oxymatrine liposomes for the alleviation of emphysema in mice via pulmonary administration, Molecules 27 (11) (2022) 3610, https://doi.org/10.3390/molecules27113610.
[32] J.Q. Peng, Q. Wang, M.Y. Guo, C.Y. Liu, X.S. Chen, L. Tao, K. Zhang, X.C. Shen, Development of inhalable chitosan-coated oxymatrine liposomes to alleviate RSV-infected mice, Int. J. Mol. Sci. 23 (24) (2022) 15909, https://doi.org/10.3390/ijms232415909.
[33] J. Shi, S.Y. Guo, Y.T. Wu, G.T. Chen, J.H. Lai, X.Q. Xu, Behaviour of cell penetrating peptide TAT-modified liposomes loaded with salvianolic acid B on the migration, proliferation, and survival of human skin fibroblasts, J. Liposome Res. 30 (1) (2020) 93–106, https://doi.org/10.1080/08982104.2019.1593451.
[34] Y.Q. Xia, C.Z. Xu, X.H. Zhang, J.K. Gao, Y.K. Wu, C.R. Li, Z.L. Wang, An activatable liposomal fluorescence probe based on fluorescence resonance energy transfer and aggregation induced emission effect for sensitive tumor imaging, Colloids Surf. B: Biointerfaces 188 (2020) 110789, https://doi.org/10.1016/j.colsurfb.2020.110789.
[35] C. Li, Q. Liu, S. Tao, Coemissive luminescent nanoparticles combining aggregation-induced emission and quenching dyes prepared in continuous flow, Nat. Commun. 13 (1) (2022) 6034, https://doi.org/10.1038/s41467-022-33857-x.
[36] Q.Y. Liu, J.W. Xue, X.R. Zhang, J.J. Chai, L. Qin, J. Guan, X. Zhang, S.R. Mao, The influence of a biomimetic pulmonary surfactant modification on the in vivo fate of nanoparticles in the lung, Acta Biomater. 147 (2022) 391–402, https://doi.org/10.1016/j.actbio.2022.05.038.
[37] X.S. Gao, Y. Xiong, H.N. Chen, X.H. Gao, J.X. Dai, Y.T. Zhang, W.H. Zou, Y. Gao, Z. Y. Jiang, B. Han, Mucus adhesion vs. mucus penetration? Screening nanomaterials for nasal inhalation by MD simulation, J. Control. Release 353 (2023) 366–379, https://doi.org/10.1016/j.jconrel.2022.11.051.
[38] C. Liu, Y.H. Liu, L. Xi, Y. He, Y.M. Liang, J.C.W. Mak, S.R. Mao, Z.P. Wang, Y. Zheng, Interactions of inhaled liposome with macrophages and neutrophils determine particle biofate and anti-inflammatory effect in acute lung inflammation, ACS Appl. Mater. Interfaces 15 (1) (2023) 479–493, https://doi.org/10.1021/acsami.2c17660.
[39] Z.W. Ye, S.F. Yuan, K.-M. Poon, L. Wen, D. Yang, Z.H. Sun, C. Li, M. Hu, H.P. Shuai, J. Zhou, M.Y. Zhang, B.J. Zheng, H. Chu, K.-Y. Yuen, Antibody-dependent cell-mediated cytotoxicity epitopes on the hemagglutinin head region of pandemic H1N1 influenza virus play detrimental roles in H1N1-infected mice, Front. Immunol. 8 (2017) 317, https://doi.org/10.3389/fimmu.2017.00317.
[40] C. Sebaaly, A. Jraij, H. Fessi, C. Charcosset, H. Greige-Gerges, Preparation and characterization of clove essential oil-loaded liposomes, Food Chem. 178 (2015) 52–62, https://doi.org/10.1016/j.foodchem.2015.01.067.
[41] K.D. Tai, M. Rappolt, L.K. Mao, Y.X. Gao, F. Yuan, Stability and release performance of curcumin-loaded liposomes with varying content of hydrogenated phospholipids, Food Chem. 326 (2020) 126973, https://doi.org/10.1016/j.foodchem.2020.126973.
[42] F. Ponti, M. Campolungo, C. Melchiori, N. Bono, G. Candiani, Cationic lipids for gene delivery: many players, one goal, Chem. Phys. Lipids 235 (2021) 105032, https://doi.org/10.1016/j.chemphyslip.2020.105032.
[43] V. Chrysostomou, A. Foryś, B. Trzebicka, C. Demetzos, S. Pispas, Amphiphilic copolymer-lipid chimeric nanosystems as DNA vectors, Polymers (Basel) 14 (22) (2022) 4901, https://doi.org/10.3390/polym14224901.
[44] G.N. He, G.F. Chen, W.D. Liu, D.X. Ye, X.H. Liu, X.D. Liang, J. Song, Salvianolic acid B: a review of pharmacological effects, safety, combination therapy, new dosage forms, and novel drug delivery routes, Pharmaceutics 15 (9) (2023) 2235, https://doi.org/10.3390/pharmaceutics15092235.
[45] N.K. Joshi, A.M. Polgar, R.P. Steer, M.F. Paige, White light generation using Förster resonance energy transfer between 3-hydroxyisoquinoline and Nile Red, Photochem. Photobiol. Sci. 15 (5) (2016) 609–617, https://doi.org/10.1039/c6pp00005c.
[46] Y. Chen, J.N. Wang, J.Z. Xu, J.Y. Zhang, S. Xu, Q. Zhang, J. Huang, J.Q. Peng, H. Y. Xu, Q.M. Du, Z.P. Gong, Fabrication of a polysaccharide-protein/protein complex stabilized oral nanoemulsion to facilitate the therapeutic effects of 1,8-Cineole on atherosclerosis, ACS Nano 17 (10) (2023) 9090–9109, https://doi.org/10.1021/acsnano.2c12230.
[47] L.M. Ensign, R. Cone, J. Hanes, Oral drug delivery with polymeric nanoparticles: the gastrointestinal mucus barriers, Adv. Drug Deliv. Rev. 64 (6) (2012) 557–570, https://doi.org/10.1016/j.addr.2011.12.009.
[48] K. Maisel, L. Ensign, M. Reddy, R. Cone, J. Hanes, Effect of surface chemistry on nanoparticle interaction with gastrointestinal mucus and distribution in the gastrointestinal tract following oral and rectal administration in the mouse, J. Control. Release 197 (2015) 48–57, https://doi.org/10.1016/j.jconrel.2014.10.026.
[49] Xabier Murgia, Paul Pawelzyk, Ulrich F. Schaefer, Christian Wagner, Norbert Willenbacher, C.-M. Lehr, Size-limited penetration of nanoparticles into porcine respiratory mucus after aerosol deposition, Biomacromolecules 17 (4) (2016) 1536–1542, https://doi.org/10.1021/acs.biomac.6b00164.
[50] G.T. Huang, S.Y. Shuai, W.C. Zhou, Y.C. Chen, B.D. Shen, P.F. Yue, To enhance mucus penetration and lung absorption of drug by inhalable nanocrystals-in-microparticles, Pharmaceutics 14 (3) (2022) 538, https://doi.org/10.3390/pharmaceutics14030538.
[51] D.A. Balazs, W. Godbey, Liposomes for use in gene delivery, J. Drug Deliv. 2011 (2011) 326497, https://doi.org/10.1155/2011/326497.
[52] M. Kendall, P. Ding, R.M. Mackay, R. Deb, Z. McKenzie, K. Kendall, J. Madsen, H. Clark, Surfactant protein D (SP-D) alters cellular uptake of particles and nanoparticles, Nanotoxicology 7 (5) (2013) 963–973, https://doi.org/10.3109/17435390.2012.689880.
[53] Q.Y. Liu, J.W. Xue, X.R. Zhang, J.J. Chai, L. Qin, J. Guan, X. Zhang, S.R. Mao, The influence of a biomimetic pulmonary surfactant modification on the in vivo fate of nanoparticles in the lung, Acta Biomater. 147 (2022) 391–402, https://doi.org/10.1016/j.actbio.2022.05.038.
[54] B. Roy, P. Guha, R. Bhattarai, P. Nahak, G. Karmakar, P. Chettri, A.K. Panda, Influence of lipid composition, pH, and temperature on physicochemical properties of liposomes with curcumin as model drug, J. Oleo Sci. 65 (5) (2016) 399–411, https://doi.org/10.5650/jos.ess15229.
[55] A. Watson, J. Madsen, H.W. Clark, SP-A and SP-D: dual functioning immune molecules with antiviral and immunomodulatory properties, Front. Immunol. 11 (2020) 622598, https://doi.org/10.3389/fimmu.2020.622598.
[56] Q.Y. Liu, J.W. Xue, X.R. Zhang, J.J. Chai, L. Qin, J. Guan, X. Zhang, S.R. Mao, Potential therapeutic applications of pulmonary surfactant lipids in the host defence against respiratory viral infections, Front. Immunol. 12 (2021) 730022, https://doi.org/10.3389/fimmu.2021.730022.
[57] S. Ding, C.L. Hackett, F. Liu, R.G. Hackett, U. Bierbach, Evaluation of a platinum-acridine anticancer agent and its liposomal formulation in an in vivo model of lung adenocarcinoma, ChemMedChem 16 (2) (2021) 412–419, https://doi.org/10.1002/cmdc.202000637.
[58] J. Wang, J. Wang, X.Z. Wang, Z. Wang, Effect of amphotericin B on the thermodynamic properties and surface morphology of the pulmonary surfactant model monolayer during respiration, Molecules 28 (12) (2023) 4840, https://doi.org/10.3390/molecules28124840.
[59] C.L. Li, J.X. Cui, C.X. Wang, J.X. Wang, Y.H. Li, L. Zhang, L. Zhang, W.M. Guo, Y. L. Wang, Lipid composition and grafted PEG affect in vivo activity of liposomal mitoxantrone, Int. J. Pharm. 362 (1-2) (2008) 60–66, https://doi.org/10.1016/j.ijpharm.2008.06.008.
[60] S.H. Alavizadeh, F. Gheybi, A.R. Nikpoor, A. Badiee, S. Golmohammadzadeh, M. R. Jaafari, Therapeutic efficacy of cisplatin thermosensitive liposomes upon mild hyperthermia in C26 tumor bearing BALB/c mice, Mol. Pharm. 14 (3) (2017) 712–721, https://doi.org/10.1021/acs.molpharmaceut.6b01006.
[61] P. Kolb, C. Upagupta, M. Vierhout, E. Ayaub, P.S. Bellaye, J. Gauldie, C. Shimbori, M. Inman, K. Ask, M.R.J. Kolb, The importance of interventional timing in the bleomycin model of pulmonary fibrosis, Eur. Respir. J. 55 (6) (2020) 1901105, https://doi.org/10.1183/13993003.01105-2019.